The Solar Cells and Their Mounting

By K. D. SMITH, H. K. GUMMEL, J. D. BODE,
D. B. CUTTRISS, R. J. NIELSEN and
W. ROSENZWEIG

Objectives in development of the solar plant for the Telstar spacecraft were to provide a power source which would withstand launching stresses and the expected space environment, with optimum end-of-life performance. Radiation damage to the silicon solar cells is the primary factor limiting their useful life; the effect of energetic protons or electrons is the generation of recombination centers in the silicon which reduce the minority-carrier diffusion length and therefore the long-wave response of the cell.

The spacecraft solar cells use the n-on-p structure, in preference to conventional p-on-n structure, to obtain a factor of 3 to 10 increased life expectancy. Response to light in the 0.4 to 0.7 micron range is enhanced by using a thin n-layer (about 0.5 micron) and an antireflection coating with minimum reflectance at 0.55 micron wavelength. Early estimates of electron and proton fluxes in the satellite orbit showed that even the best cells would not give sufficient life without radiation shielding. Therefore the cells are protected against electrons of energy up to 1 Mev by 0.3 gm/cm² sapphire cover plates. The cell mountings are designed to withstand peak vibration stresses of 200 g and repeated temperature cycles from +65°C to −100°C.

The 3600-cell solar power plant is composed of 300 twelve-cell groups of 1 cm × 2 cm cells, yielding a nominal initial power of 14 watts at 28 volts for any spin-axis orientation relative to the sun. Telemetry information on performance of the solar plant indicates degradation of the shielded solar cells equal to that measured in the laboratory on unshielded cells with a 1-Mev normal incidence flux of 6 × 10¹² electrons/(cm² day). From this comparison it is estimated that the plant will degrade to 68 per cent of its initial output after two years in orbit.

I. INTRODUCTION AND BACKGROUND

1.1 Introduction

General objectives in design of the solar plant for the Telstar spacecraft were to provide cells and mounting arrangements suitable for

prolonged operation in a radiation environment and, consistent with the state of technology and the program schedules, to optimize the output per cell after some years in orbit. Preliminary estimates clearly indicated that deterioration of cell output through energetic particle radiation damage would be the most serious effect, and that, unless this damage could be held within reasonable bounds, we would be forced to over-design the initial power considerably, perhaps by a factor greater than two, as compared to end-of-life requirements. Answers to the following questions were urgently needed:

(1) What power must be supplied by the solar plant?

(2) What orbit will be used?

(3) What radiation will be encountered?

(4) What will be the effect of this radiation on the solar cells?

(5) What design choices may be made and how do they interact to affect life?

(6) What other factors are of importance besides radiation effects?

(7) What temperatures and temperature gradients must be designed for?

(8) Can manufacturing feasibility be shown for structures of optimum or near-optimum design?

This report will consider: the radiation effects study; design, fabrication and evaluation of the solar cells; design and engineering of the mounting of solar cells into groups; mounting and arrangement of cell module groups on the satellite; performance estimates and measurements leading to the choice of total number and connection of cells; and measurements of performance. It begins with consideration of the historical background of the solar cell and ends with evaluation of the flight performance.

1.2 *Background*

Silicon photovoltaic converter cells of moderate-to-high solar conversion efficiency were first prepared in 1954.[1] In the following two years, a few cells with 11 per cent conversion efficiency were made, and in the laboratory it became possible to fabricate cells in the 8 per cent to 10 per cent range with good yield.[2] The process was at this time given to Bell System licensees, some of whom continued development through the next several years.

In the early development, cells of both p-on-n and n-on-p structure were made. However, during the greater part of the development program n-type silicon of appropriate resistivity was more readily available

than p-type; also, the p-on-n cells made at that time gave somewhat higher conversion efficiency than n-on-p cells — perhaps because of the low reflectance of the degenerate surface layer characteristically resulting from the boron trichloride diffusion process. The result was that the standard or conventional solar cells made in the U. S. have been of the p-on-n structure. Russian development engineers, and possibly others in Europe, appear to have concentrated on n-on-p cells, perhaps because of material availability or the state of their diffusion technology, or both.

3.1 *Principles of Operation*

A brief discussion of the operation of the solar cell is in order as an introduction to more detailed consideration of the merits of different cell structures and effects of radiation and other environmental factors. The silicon photoelectric energy converter or solar cell, shown schematically in Fig. 1, is representative of a class of devices in which radiant energy is absorbed within a material, thereby upsetting an equilibrium condition and permitting electrical power to be delivered to an external circuit. In the solar cell, the absorbed photons create electron-hole pairs in the silicon. In the frequency range of interest, one pair is produced for each photon.

Referring to Fig. 2, it can be seen that events subsequent to the arrival of photons at the cell surface may be:

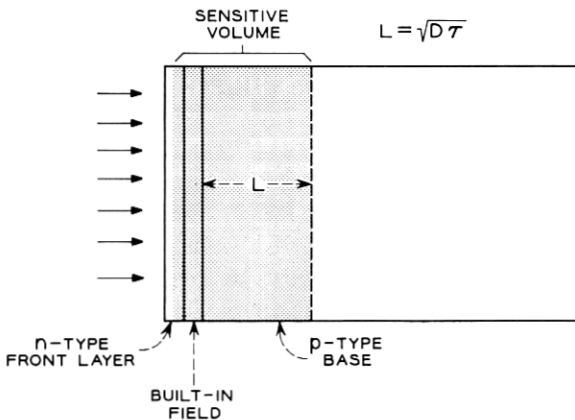(1) Photons are reflected and thus no energy is available.
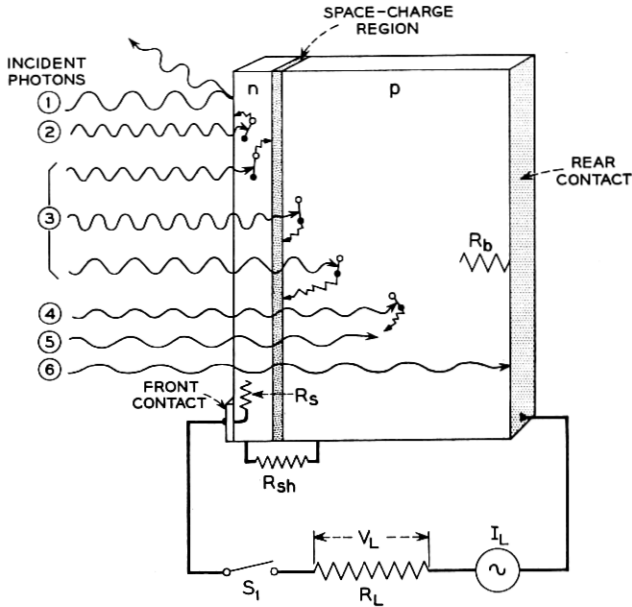

Fig. 1 — Schematic of n-on-p solar cell.

Fig. 2 — Photon and resistive losses.

(2) Photons are absorbed near the cell surface, creating hole-electron pairs, but the holes recombine with electrons without reaching the field region at the p-n junction. No electric energy is available from this reaction; however, thermal energy appears.

(3) Hole-electron pairs are created near enough to the junction for the minority carrier to reach the field region and cross the junction, contributing to the useful output current. Some heat is also generated.

(4) Pairs are created, but too far from the junction to be useful.

(5) Photons are absorbed, but have insufficient energy to create hole-electron pairs. Only heat is generated.

(6) Low-energy photons may not be absorbed in the semiconductor.

Since only the photons of (3) are effective in contributing to the electrical output of the cell, every effort will be made to optimize conditions so as to make use of as many photons as possible.

The external power which can be generated by the charge carriers which reach the junction is affected by the following considerations:

(a) The terminal voltage of the device cannot exceed that value which will drive across the junction a forward current equal to the photon-generated current. If we consider the situation with switch S_1 of

Fig. 2 open, we see that the forward bias current will just equal the generated current; the efficiency will then be zero.

(b) The generated current must flow to the external circuit through the series resistance R_s of the diffused layer and the series resistance of the semiconductor body, R_b. Generally, the body resistance can be made much lower than the surface layer resistance.

(c) There will be some shunt resistance, R_{sh}, effectively in parallel with the p-n junction. Generally this may be neglected in power circuits.

From the above discussion, it becomes evident that performance optimization will require consideration of:

(1) the spectral distribution of solar radiation
(2) the environment
(3) the properties of the semiconductor
(4) reflection losses
(5) recombination losses
(6) parasitic resistive losses
(7) load impedance and
(8) the useful life desired — if the environment is destructive.

1.4 *Significance of Van Allen Belt*

Before 1957, estimates of expected life of satellite solar power plants did not generally include deterioration of performance resulting from energetic particle radiation, since no continued high-intensity source was known and the integrated effects from cosmic rays and solar flares were not expected to be serious. The discovery of the Van Allen belts[3] changed this situation completely. For satellites at altitudes in the 1000–10,000-mile range, particle radiation is the principal cause of solar cell performance loss. Therefore, it became of immediate importance to evaluate the radiation effects and, if possible, design solar cells and solar power plants to be radiation resistant. A development program initiated at U. S. Army Signal Research and Development Laboratories (USASRDL), with the objective of obtaining solar cells of improved conversion efficiency, had resulted in a feasibility demonstration of n-on-p cells comparable in conversion efficiency to the p-on-n cells commercially available in 1960. Also, these cells had a thin n layer, so they were more sensitive in the short-wave end of the visible spectrum and better matched to space sunlight than conventional cells.

In the course of radiation evaluation experiments[4] on USASRDL cells conducted by Radio Corporation of America under NASA contract, these n-on-p cells were found to be significantly more resistant to both

electron and proton radiation than p-on-n cells of equivalent initial performance. On December 8, 1960, USASRDL presented their results, together with a complete description of their laboratory scale fabrication operations for the n-on-p cell, to representatives of the major industrial laboratories.

Bell Telephone Laboratories development effort on the radiation-resistant n-on-p cell was initiated in October, 1960, as a result of the early radiation reports[5,6] and informal discussion with Signal Corps personnel. Some of the Laboratories staff assigned to this development had also engaged in the p-on-n cell feasibility development (1955–56), and so had considerable experience in solar cell technology. Laboratory fabrication of n-on-p cells was undertaken about the end of October, 1960, and the first cells exhibiting satisfactory performance were made about a month later.

1.5 Solar Cell Requirements for the Telstar Spacecraft

During the early part of the n-on-p solar cell development, and even into the initial Western Electric Co. fabrication, the satellite power requirements were not firm and the number of cells to be used on each vehicle was not known. The objectives were to achieve the highest end-of-life performance consistent with manufacturing feasibility. Having established this performance level, the total number of cells required for a particular end-of-life power requirement could be determined to the accuracy with which the environmental conditions could be predicted. Coordinated work on evaluation of radiation effects, technology of cell fabrication, environmental studies, and satellite power drain was therefore required. This work is considered in the following sections.

II. RADIATION DAMAGE STUDIES

2.1 Background

Proton and electron particle radiation, such as is found in the Van Allen radiation belts, produces permanent damage in silicon by reduction of the minority-carrier lifetime. This degrades the solar cell performance by decreasing the collection efficiency for carriers generated by penetrating light and by increasing the saturation current of the junction. The degradation of lifetime with particle bombardments of the type and energy expected in the Van Allen belts is thus of primary interest, as is the correlation between the performance of a given type of solar cell and its bulk minority-carrier lifetime.

The type of information on radiation damage in semiconductors available at the beginning of the project is quite well summarized in Ref. 7. Work on damage rates for protons had been almost nonexistent (the nature of the defect was considered too complex to allow simple analysis), and the electron damage studies had emphasized the search for the location of energy levels in the forbidden gap. All evaluations of the defect introduction rates had indicated that the results were dependent on the presence of impurities, both controlled and uncontrolled. Electron spin resonance experiments carried out since that time have indicated that the important defects, at least in n-type silicon, arise from complexes of vacancies in association with impurity atoms.

In light of this situation the radiation damage problem was approached with the following objectives:

(1) the evaluation of the outer space solar cell performance on a good statistical sample of cells bombarded by a convenient source of radiation (1-Mev electrons) and the correlation of this performance with the minority-carrier lifetime;

(2) the determination of lifetime degradation rates for protons of various energies and for electrons of various energies and under various shielding thicknesses; and

(3) the synthesis of the above information for the best available Van Allen belt spectrum with the assumption of "equal performance for equal lifetime" for a specific type of cell.

2.2 *Measurement Techniques*

The most important parameter characterizing the outer space performance of the solar cell is its outer space short-circuit current. Once this quantity has been accurately determined, the output characteristics can be measured under any convenient light source whose intensity has been adjusted to produce the predetermined outer space short-circuit current.

Determination of outer space short-circuit current was carried out by measuring the response of the cells at various discrete wavelengths and using this information to synthesize the outer space cell response.[8] The synthesis is achieved by multiplying the response at a given wavelength by an appropriate weighting factor, so that the summation of these products over all wavelengths yields the integral which represents the outer space short-circuit current. This procedure also allows one to assess the contributions to the total current of the various wavelength components, and thus to optimize the design in regard to spectral response.
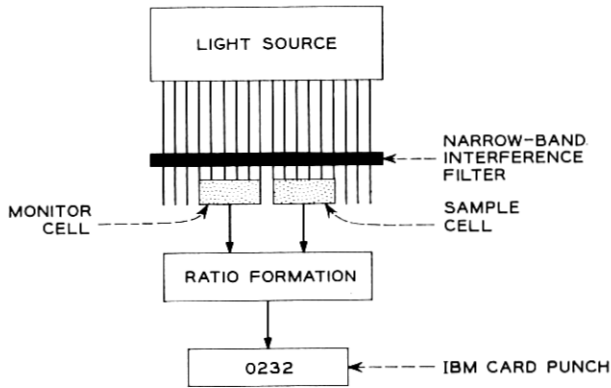
Fig. 3 — Schematic representation of spectral response ratio measuring apparatus.

An automatic test set was developed[9] which carries out spectral response measurements at eight wavelengths, in addition to making five other tests which serve to evaluate the cell junction characteristics. Fig. 3 shows schematically the method used for measuring the spectral response. Electronic ratio formation of the response of the sample relative to the monitor cell is used to eliminate the influence of fluctuations and aging in the light source. All measurements appear in digital form and are punched on IBM cards to permit further processing.

The minority-carrier lifetime was determined by measuring a related parameter, the minority-carrier diffusion length. Diffusion length measurements were carried out by a technique which utilizes the ionizing properties of penetrating radiations such as high-energy electrons, protons, and gamma rays.[10]

2.3 1-Mev Electron Statistical Experiment[11]

A statistical evaluation of solar cell performance was carried out with a 1-Mev electron Van de Graaff generator. Groups of 16 or more solar cells of the following types were used:

(1) Blue-sensitive n-on-p cells produced by Western Electric Co.: these cells were randomly selected from a lot of 10,000 cells, from which only those cells having an efficiency less than 7.5 per cent under outer space light had been removed.

(2) Normal p-on-n cells secured from a commercial source and rated as 14 per cent efficient under tungsten light.

(3) Blue-sensitive p-on-n cells secured from a commercial source and rated as 12 per cent efficient under outer space light.

To achieve uniform exposure for all cells, the solar cells were mounted near the perimeter of an aluminum disk, which was continuously rotated during the irradiations in such a way that the cells passed through the center of the beam.

The cells were irradiated in five steps to integrated fluxes of 1.8×10^{13}, 9.0×10^{13}, 5.4×10^{14}, 2.7×10^{15} and 1.8×10^{16} electrons/cm². Before the first and after each successive bombardment the cells were subjected to optical and electrical measurements and to measurements of the minority-carrier diffusion length. The results of the experiment are shown in Figs. 4, 5, and 6. Fig. 4 is a plot of the outer space short-
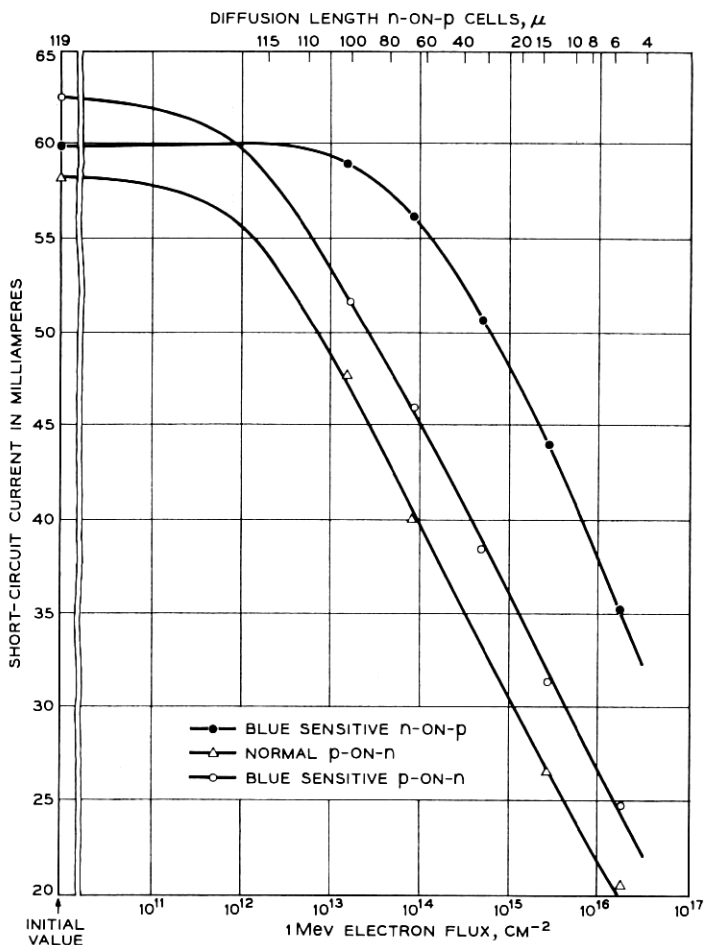

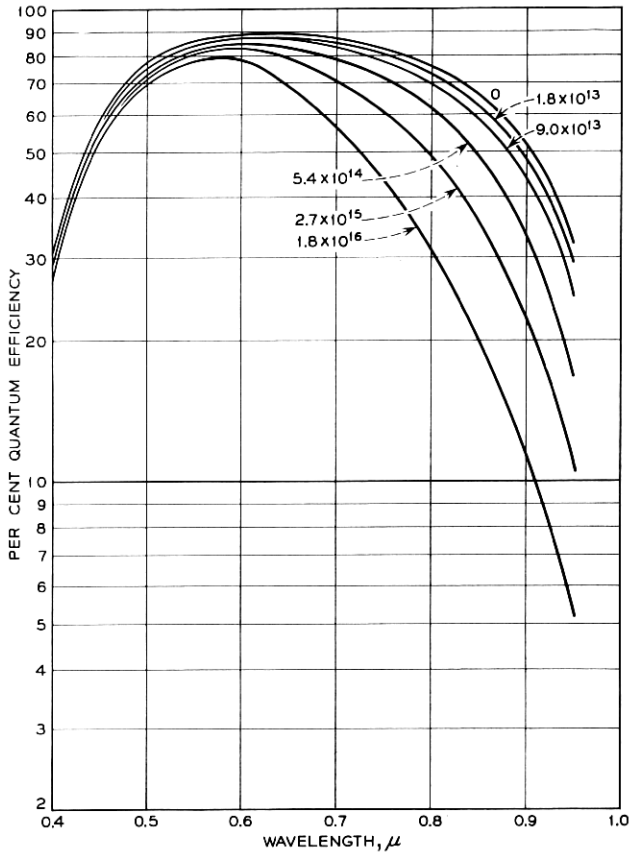Fig. 4 — Outer space short-circuit current as a function of 1-Mev electron flux.

Fig. 5 — Per cent quantum efficiency as a function of wavelength for n-on-p cells, with 1-Mev electron flux as parameter.

circuit current as a function of bombardment flux. A detailed analysis[11] shows that the short-circuit current degradation is consistent with the diffusion length degradation and its effect on the quantum efficiency. Fig. 5 is a plot of the per cent quantum efficiency, defined as the number of carriers collected per 100 incident photons of a given wavelength, as a function of wavelength for various levels of bombardment of the n-on-p cells.

The predicted maximum power for outer space sunlight as a function of flux is given in Fig. 6. The decrease in maximum power with bombardment is caused not only by the decrease in short-circuit current but also by the degradation of the junction characteristics.
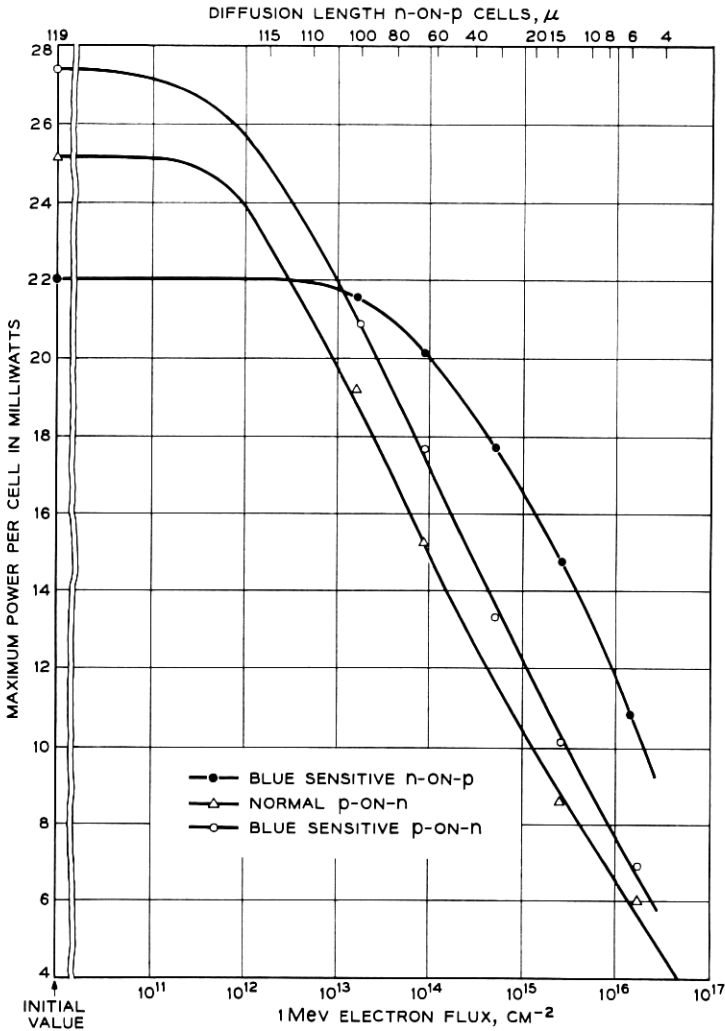
Fig. 6 — Outer space maximum power as a function of 1-Mev electron flux.

2.4 *Proton Bombardments*[12]

The proton bombardment damage study of solar cells required the use of four accelerators for coverage of the energy range of interest. At the higher-energy accelerators, the solar cells were stacked with aluminum absorbers to allow a simultaneous exposure at energies ranging from the initial beam energy down to about 20 per cent of this value.

The ionizing property of the proton beams was used to monitor the radiation-induced diffusion length changes. This change was found to follow quite closely the formula

$$\frac{1}{L^2} = \frac{1}{L_0^2} + K\Phi \tag{1}$$

in which Φ is the bombardment flux in cm^{-2}, L is the diffusion length in cm for that flux, and L_0 is the initial diffusion length. The damage coefficient, K, can thus be determined as a function of proton energy in these experiments. The damage coefficient, K, is a measure of the damage rate for a given type of radiation on the cell. The relative fluxes of two different radiations to produce the same damage may be obtained by forming the inverse ratio of their damage coefficients.

The results are summarized in Fig. 7, which is a plot of K vs proton energy. The K values appearing in the figure are those which are observed after two weeks of room temperature annealing, which results in a recovery of about 15 to 20 per cent in diffusion length. Relative K values were also obtained for one set of 1 ohm-cm p-on-n cells in the energy range 16.8 Mev to 130 Mev, and were found to be greater by a factor of 6.2 ± 2 independent of energy.
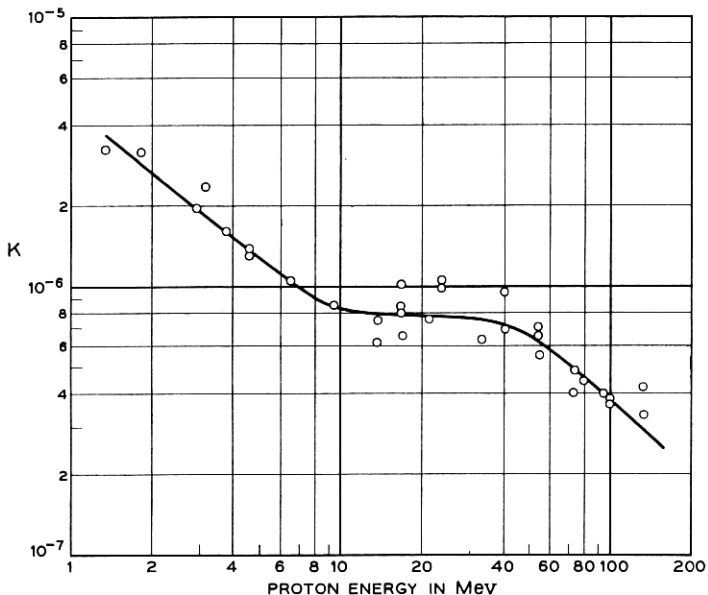

Fig. 7 — Damage rate as a function of proton energy.

2.5 *Original Estimates of Solar Plant Radiation Damage*

During the design phase, the data available for estimating the Van Allen belt radiation fluxes were quite limited. An integral omnidirectional proton spectrum was estimated by constructing a composite curve which above 40 Mev had a slope as determined by Freden and White,[6] and at lower energies as determined by Naugel and Fichtel.[13] Such a curve was made to pass through Van Allen's[3] point, 2×10^4 cm^{-2} sec^{-1} at 40 Mev for the heart of the belt. The resulting omnidirectional integral spectrum is shown in Fig. 8. For protons, the effect of shielding can be taken into account readily by making use of the range-energy relationship to calculate the energy attenuation. The result of shielding calculations is given as the upper curve in Fig. 9. The calculation is based on the proton spectrum of Fig. 8 and expressed in terms of an equivalent 1-Mev electron flux that would cause equal damage when normally incident on unprotected cells. This curve shows that the damage is reduced by a factor of about 10 when the shielding thickness is increased from 0.1 to 0.3 gm/cm². The relatively smaller advantage with larger shielding thickness is mainly due to the hardening of the proton spectrum for energies above 40 Mev. The shielding thickness used on the Telstar spacecraft is about 0.3 gm/cm², in the form of 30 mils of sapphire.

The electron component was estimated from Van Allen's[3] measurements, which indicated for the heart of the inner belt omnidirectional
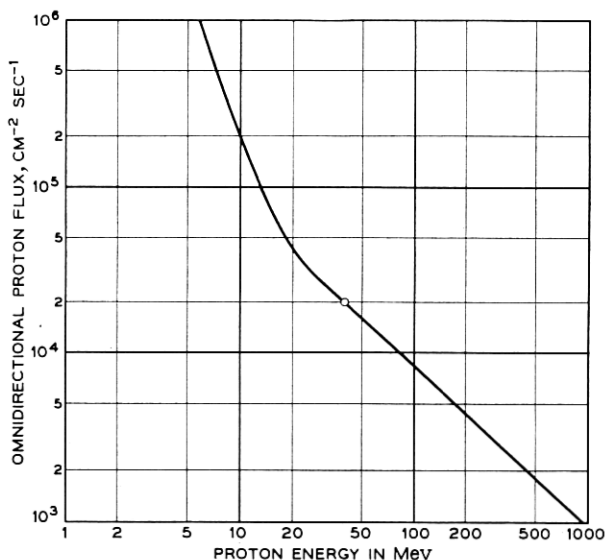

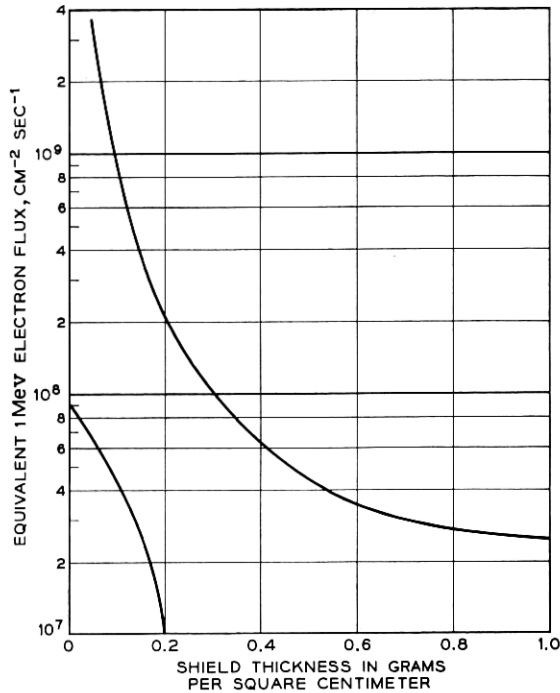Fig. 8 — Omnidirectional integral proton flux as a function of energy.

Fig. 9 — Equivalent 1-Mev electron flux as a function of shielding thickness.

intensities of 2.5×10^{10} cm^{-2} sec^{-1} for energies greater than 20 Kev, and 1×10^8 cm^{-2} sec^{-1} for energies greater than 600 Kev. Cells covered with various thicknesses of sapphire were subjected to electron bombardments at a set of energies (0.4, 0.6, 0.8 and 1.0 Mev) with intensities designed to simulate the above spectrum. The resultant equivalent 1-Mev flux as a function of shielding thickness is also shown in Fig. 9. According to these data, the electron damage is small compared to the proton damage. However, in view of data taken after the July 9, 1962, high-altitude nuclear test explosion, the equivalent fluxes of Fig. 9 are not applicable to the satellite which was launched on July 10, 1962. In Section 5.6, the flight performance of the solar plant will be discussed in the light of our present understanding of the radiation belts.

III. CELL DESIGN AND FABRICATION

3.1 *Considerations Leading to Decision to Develop N-on-P Cells*

During the fourth quarter of 1960, the superiority of n-on-p over p-on-n silicon cells in high-level radiation environments was firmly

established. Cells of the n-on-p type are more resistant than p-on-n cells to 1-Mev electron irradiation by a factor of as much as ten. They are also from 3 to 8 times less sensitive to protons than p-on-n cells in current use.

At that time, there were no n-on-p silicon cells in production in commercial quantities. However, experimental n-on-p cells were obtained from several suppliers, and information was made available by the Signal Corps on methods of fabrication of n-on-p cells. This information, combined with our own development studies, led to the conclusion that the n-on-p cells would not be essentially more difficult to manufacture than p-on-n cells of comparable initial performance in space, except that (a) an antireflection coating would be required, which was not necessary as a separate operation on the p-on-n cell, and (b) development effort would be required to obtain a highly manufacturable electrical contact of good integrity and low electrical resistance. We concluded that these problems could be solved and that a suitable cell could be nearly as economical in quantity fabrication as p-on-n cells of comparable initial performance in space. The decision to initiate the n-on-p cell program was based on the two prime considerations: (1) the cells would give longer life in a radiation environment, and (2) they appeared feasible for manufacture.

3.2 N-on-P Solar Cell Design

3.2.1 Material

Silicon material characteristics usually considered important in semiconductor work are (1) the impurity concentration or doping level, (2) the minority-carrier lifetime, (3) the crystal structure perfection, and (4) the crystallographic orientation. For solar cell fabrication, the size of the crystal may also be a consideration, particularly if cells are to be carried through several fabrication steps as multiple elements.

For n-on-p cells for satellite service, the effects of changes or variations in these characteristics required evaluation. Silicon was obtained from several sources over a range of resistivity for comparative process evaluation. Since the prime effect of the radiation environment on the cell is a reduction in carrier lifetime, there appeared to be no advantage in requiring high initial lifetime in the starting material, or extreme perfection of structure. Therefore, during the period of manufacture, the silicon material used by Western Electric Co. for this project was not held to a stringent lifetime requirement, nor were the imperfections controlled by monitoring the etch pit count. The crystals were sliced parallel to the

[111] crystal plane, and twinned material was rejected for mechanical reasons. It was found feasible to grow crystals of sufficient diameter that one-inch square slices could be cut. These were used as the starting material for cell fabrication. One hundred or more such slices were usually cut from a single crystal.

The impurity concentration in the cell body, which determines the specific resistivity, can affect the cell voltage, the sensitivity to radiation damage, and the effective series resistance of the cell. This last effect is small in the range of resistivity usually used: it would reach 0.1 ohm with a body resistivity of 5 ohm-cm. The envelope of open-circuit voltage measurements vs material resistivity obtained with experimental cells is shown in Fig. 10. As expected from theoretical considerations, better radiation resistance would be obtained with high-resistivity silicon used as starting material. However, the loss in open-circuit voltage obtained with experimental cells of high resistivity silicon led to a decision to use nominal 1 ohm-cm p-type silicon for the initial production, and this was continued through the program.

3.2.2 Cell Structure

Early in our development program, a decision was made to keep the physical dimensions of the cells compatible with commercially available p-on-n cells, if this could be done without serious sacrifice in performance. Fig. 11 shows the cell dimensions and front contact arrangement. The cell was made about 5 mils thinner than the conventional product; this resulted in a minor weight saving without serious loss in strength.

An etch-polished front surface was adopted to reduce surface recombination losses and permit application of a smooth antireflection
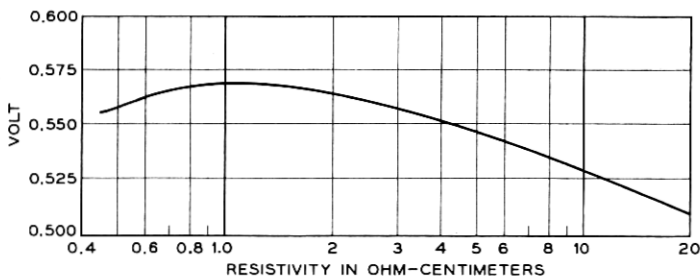

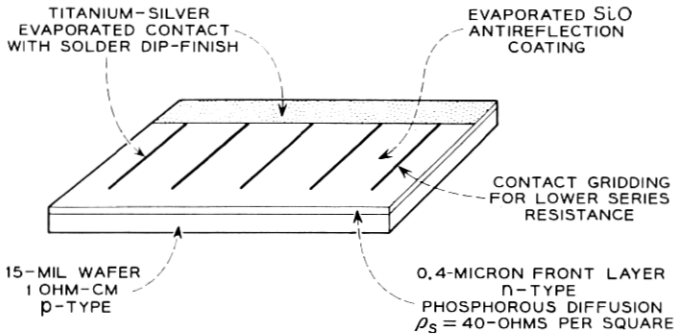Fig. 10 — Solar cell open-circuit voltage vs resistivity.

TITANIUM-SILVER   EVAPORATED SiO
EVAPORATED CONTACT   ANTIREFLECTION
WITH SOLDER DIP-FINISH   COATING

                                                   CONTACT GRIDDING
                                                   FOR LOWER SERIES
                                                   RESISTANCE

15-MIL WAFER   0.4-MICRON FRONT LAYER
 I OHM-CM   n-TYPE
 p-TYPE   PHOSPHOROUS DIFFUSION
                                     $\rho_S = 40$-OHMS PER SQUARE

Fig. 11 — Cell structure.

layer of uniform thickness. Good adhesion and integrity of this antire-
flection coating required coordinated effort on the diffusion process,
postdiffusion cleaning, and the contact application process, which is dis-
cussed in more detail in Section 3.3.

The diffusion process was selected after a series of diffusion experi-
ments, combined with contact studies and model fabrication. Control of
the diffusion operation was used as the principal method of adjusting
the spectral response of the cell. The control was exercised by require-
ments placed on the diffusion environment and temperature, leading to a
specified n-layer sheet resistance and desired n-layer thickness.

The cells were designed to be sensitive in the blue-green region of the
solar spectrum. No particular efforts were made to obtain good long-
wave response since, as discussed in Section II, the long-wave or infrared
response is degraded rapidly in a radiation environment. The photon
sensitivity peak was chosen to be near the wavelength for maximum
incident photon flux from the sun. Fig. 12 shows calculated short-circuit
current response, initial quantum efficiency, and relative response
for equal energy input vs wavelength for a typical n-on-p cell after anti-
reflection coating.

At the start of the development program, it was realized that improved
cell contacts would be required. Intensive work was initiated, leading
to the titanium-silver evaporated contact used on all Western Electric
Co. n-on-p cells. This in turn required special attention to the solder
used for cell tinning and assembly. Many experiments were made to
determine optimum methods for assembling the cells in series groups, as
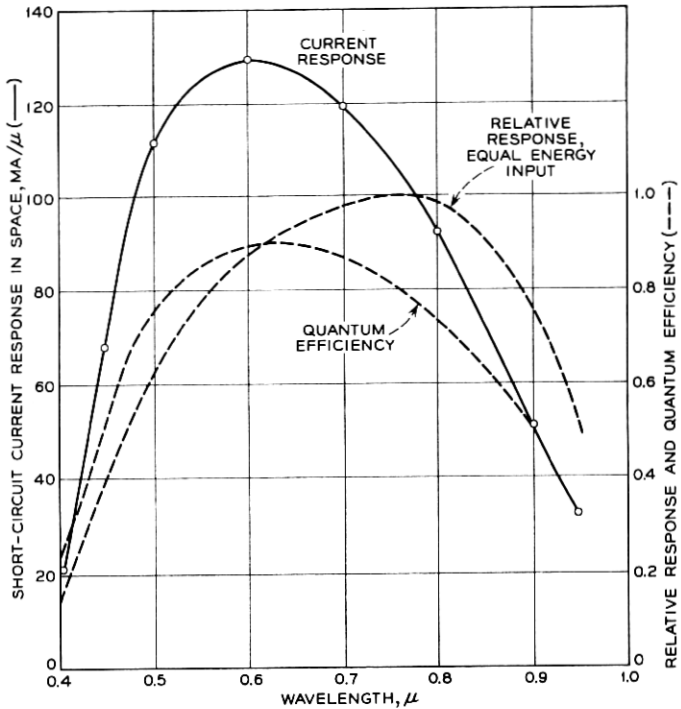will be considered in Section IV.

Fig. 12 — Spectral response, n-on-p solar cell.

3.3 *Fabrication Technology for N-on-P Cells*

3.3.1 *General*

This section describes some development experiments and the fabrication methods for making radiation resistant solar cells. During the period October 1960–June 1961, a moderate scale model fabrication operation was conducted in the laboratory. This model line was used for design experiments and to provide cells of specified characteristics for radiation damage study. The "going rate" was a fabrication of about 100 cells per week, and a total of some 2000 experimental cells was made in this period in the laboratory.

The first cells were delivered to the Laboratories by Western Electric Co. on January 28, 1961, and the desired program was completed about March 30, 1962. A total of approximately 100,000 n-on-p cells was made by Western Electric Co. for the program; however, not all of these re-
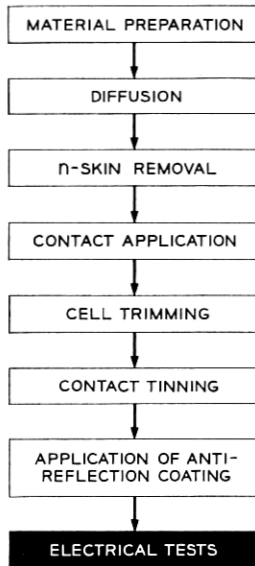
Fig. 13 — Fabrication sequence for n-on-p solar cells.

ceived antireflection coatings, and not all of those coated were considered acceptable for satellite use.

Fig. 13 indicates the principal steps in our fabrication of n-on-p solar cells. These steps are considered in sequence, and some of the development experiments and analyses leading to the final cell are mentioned. Since no n-on-p cells were in quantity manufacture (in the U. S. A.), considerable development engineering was required. Also, the time schedule for manufacture required that equipment and facility orders be placed on the basis of advance engineering judgment, without the benefit of a "proved in" process. Fortunately, it was not necessary to scrap any major equipment as the fabrication methods became shaken down.

3.3.2 Silicon Material and Preparation

3.3.2.1 Material. The material specified for the Telstar cells was p-type single-crystal silicon, sliced parallel to the [111] crystal plane with resistivity 1.0 ± 0.50 ohm-cm and minority-carrier lifetime greater than 5 μsec. No requirement was placed on etch pit density. The silicon slices were cut from the parent crystal with a multiple gang saw to a thickness of 20 mils, minimum. The slice was made 1.0 inch square (nominal),

in order that two cells could be prepared on one slice of the starting material. The crystals were pulled approximately one and one-half inches in diameter and from four to five inches long.

In laboratory experiments, material of resistivity in the range 0.05–20 ohm-cm was used. Several experimental fabrications were made, with material of different resistivity processed through the same operations at the same time to reduce the number of independent variables and establish the effects of material resistivity on cell performance. As previously indicated, optimum initial performance was obtained with silicon near 1 ohm-cm, and this was specified.

Silicon material was usually pulled into single-crystal form by Western Electric Co.; however, some single-crystal stock was obtained from other material suppliers and used for comparative fabrication. Little difference in cell performance was found attributable to the source of the single-crystal starting material, and for most of the operation no restrictions were placed on the source of the material used.

Experiments were also made in which solar cells were fabricated from twinned material, both with a single grain boundary and with many grain boundaries indicated on a cell. No significant deterioration in electrical performance was found until the number of grain boundaries became very large (of the order of 100), so that the material would more properly be called "multicrystalline, with large grain size" than "single-crystal, twinned." However, silicon slices showing grain boundaries were rejected for satellite use because of their inferior mechanical strength.

3.3.2.2 *Slice Preparation.* After the crystal was sawed into slices, the slices were lapped on both sides, and then one side was etch-polished; about three mils of material were removed by the etch. The slices were demounted from the etching racks, cleaned, and inspected for stains, scratches, and mechanical dimensions. The purpose of the etch-polishing step was to provide the best possible surface for the diffusion operation, to avoid crystal imperfections in the finished cell which would cause high surface recombination, and to facilitate application of an effective antireflection coating. A "modified CP4" type etch was usually used. To obtain consistent results, both the bath temperature and the agitation were carefully controlled.

3.3.3 *Diffusion, N-Skin Removal*

The diffusion process used for preparation of the thin n-layer is shown schematically in Fig. 14. This was chosen only after extensive development experiments using different methods of application, time-tem-
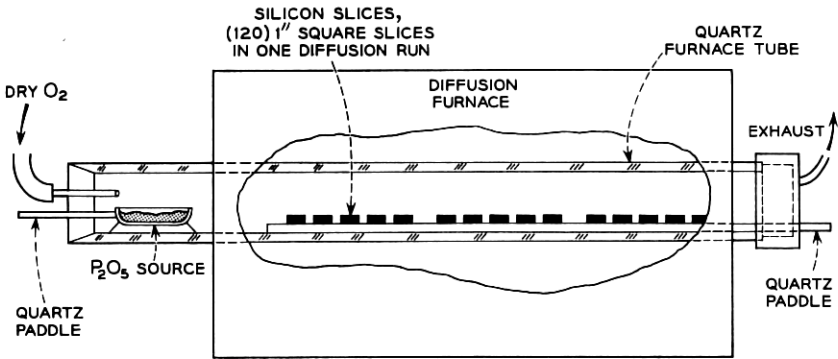
Fig. 14 — Schematic of phosphorus diffusion system.

perature programs, and sequences of operations. Significant factors in control of the diffusion process were found to be: cleanliness of silicon samples, temperature and quantity of the P_2O_5 source, method of introducing source and carrier gas, velocity of carrier gas flow, cleanliness of quartz trays and, of course, the time and temperature of the diffusion.

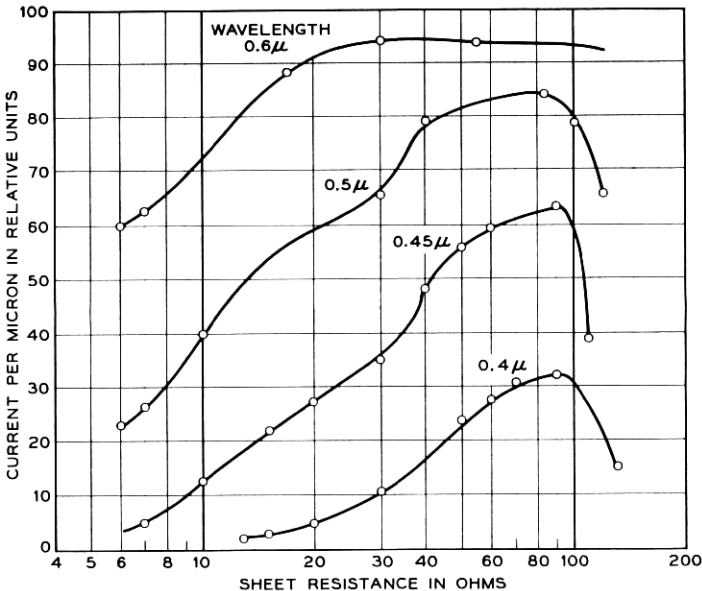Fig. 15 shows the response of experimental (pre-antireflection-coated)

Fig. 15 — Spectral response vs sheet resistance.

cells vs the measured sheet resistance of the diffused layer at four wave-lengths in the visible range. For these cells, it would at first appear that the optimum diffused layer sheet resistance would be about 90 ohms/square; however, attempts to fabricate cells in quantity with such thin diffused layers showed that further development would be required to obtain reasonable yields. A principal difficulty was local shorting of the cell in later process steps, particularly in contact application. As a compromise, the sheet resistance of production cells was specified to be greater than 30 and less than 60 ohms/square. The diffusion time and temperature were programmed to produce a diffusion depth in the order of 0.4–0.5 micron, with sheet resistance of perhaps 37 ± 5 ohms/square. As the diffusion depth was not subject to accurate measurement in the slightly irregular surface provided by the etch-polishing operation, this was not held as a requirement.

After diffusion and postdiffusion inspection, the n-skin was removed from the lapped side of the slice by a light abrasive blast, or by etching. Considerable care is required at this step, as the thin n-p junction on the polished face is quite sensitive to local damage if roughly handled in the presence of abrasive particles. It was found expedient to mask the face of the slice during the blasting or etching operation, as by cementing or waxing to a glass cover slide.

3.3.4 *Contact Application*

Adherent, low-resistance contacts to the n and p regions of the n-on-p solar cell presented a major problem. Electroless nickel plating followed by sintering would make a satisfactory mechanical connection, but was unacceptable for the n-layer, as the very thin diffused region would be penetrated during the sintering, and the n-p junction would be seriously degraded, if not shorted entirely. A new approach was needed. After some study, effort was concentrated on development of a new semiconductor contact, in which a reactive metal, titanium, is applied to the silicon surface in vacuum, and the titanium is covered with silver before removal from the vacuum chamber. The silver serves to protect the titanium from oxidation and permits ready tinning at a later point in the fabrication.

Silicon is normally covered with a thin SiO_2 layer, which is one cause of difficulty in forming good electrical contacts to it. In the titanium-silver contact process, the titanium is applied to this thin oxide layer. After removal from the vacuum station, the silicon slices are baked for a few minutes in an inert atmosphere at a temperature near 600°C.

During this heat treatment, the titanium reacts sufficiently with the SiO₂ surface layer to penetrate it and make electrical contact to the underlying silicon. This forms an adherent, low-resistance contact, without forming any liquid alloy and without damage to the n-p junction. If the surface is clean and if the vacuum deposition is properly carried out, the metal-silicon bond is very good. For example, if a heavy wire lead is soldered along the back of the cell and the combination is immersed in liquid nitrogen, thermal contraction differentials will rip the wire from the silicon body. However, the parting line is usually not at the metal-silicon interface, but rather inside the silicon. Because of the good electrical and mechanical properties of the Ti-Ag contact, it was used for both front and back contacts on all Telstar spacecraft cells.

Accessory contact "grid lines" or "fingers" are necessary on high-efficiency solar cells to reduce ohmic losses in the thin surface layer. This becomes more important as the diffused layer is made even thinner to optimize short-wave spectral response, as required for use in a radiation environment. However, the number of fingers should not be made too large, as the light which they intercept does not contribute to useful output. A compromise must be made. The "best" choice of finger array will depend on the width of the fingers, the cell geometry, and particularly on the diffused layer sheet resistance. For the Telstar space-craft cell, five fingers were used. Experimental cells, fabricated alike up to the point of contact application, but made with both five fingers and seven fingers (each 0.006 inch wide) showed little difference in perform-ance. If the sheet resistance of the diffused layer were increased, say to 60–80 ohms/square, then seven-finger cells would be preferred.

3.3.4.1 *Relief of Back Contact Margin.* The cells made early in the program had the rear contact applied over the entire rear surface of the slice. After assembly of several modules and thermal shock tests, it was found that small cracks would sometimes become evident at or near the edge of the cell beneath the top contact. This was attributed to strains set up by the solder and the metal mounting strip, these being attached directly to the bottom of the cell at the edge. Several means for avoiding this strain concentration were examined. The method adopted was to mask a narrow region along the edge of the cell, so that during evaporation of the rear contact this region would not be metal-lized and therefore, would not "take" solder. This operation required registration of front and back contact evaporation masks, however.

3.3.4.2 *Contact Adherence Tests.* After contact evaporation and heat treatment, the contacted slices were subjected to a "Scotch Tape" ad-herence test in which a strip of pressure-sensitive tape was applied to

each slice and stripped away. Defective contact adherence was shown by portions of the silver or silver and titanium adhering to the tape. Such slices were rejected at this point without further process effort.

3.3.5 *Cell Trimming and Tinning*

To this point in the process, two 1-cm × 2-cm cells have been prepared on a single silicon slice. These cells are now cut apart with a ganged diamond saw, which also trims the other edges of the cell to final dimension. Fig. 16 shows top and bottom views of the contacted slice with the trimming cuts. It will be evident that the width of the saw kerf in the cut which separates the cells must be allowed for in dimensioning the contact evaporation masks.

By trimming the cells on their entire perimeter after the contact application, any metallization across the exposed n-p junction is avoided. Also, some simplification of operations results from handling the cells as multiples of two through part of the fabrication. The cells, after trimming, are demounted from the cutting block, cleaned, and solder-tinned. This operation is done by dipping each cell in a bath of molten solder in an inert atmosphere. The solder contains about 3 per cent silver to prevent dissolving the silver already present on the cell. Some control of the amount and location of the solder on the rear face of the cell is available by adjustment of solder temperature, time of immersion, and method of removal of the cell from the solder bath. After tinning, the
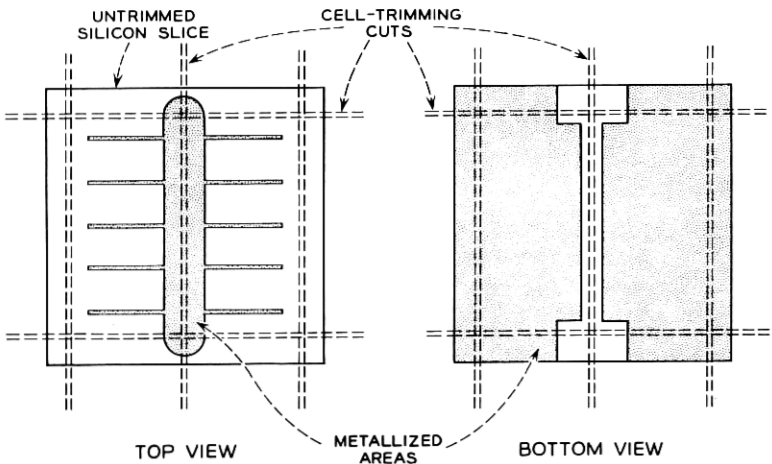

Fig. 16. — Contact configuration and cell trimming.

cells are cleaned with acetone and are delivered for preliminary electrical tests.

In our program, the edges of the cell were not given any etching or smoothing treatment after the diamond saw trimming operation. It was originally planned to provide some form of etch treatment to remove material damage introduced in sawing; however, experiments indicated that little improvement was obtained. The thin n-p junction is highly susceptible to mechanical damage on the face of the n-layer but is rather tolerant of damage at the exposed perimeter (6 cm) of the cell. The relative importance of etching the junction perimeter appears to diminish as the diffused layer is made very thin.

3.3.6 *Preliminary Electrical Tests*

Before application of the antireflection coating, the cells were subjected to electrical tests. All cells were tested for open-circuit voltage, short-circuit current, current into 0.45-volt load, reverse leakage current, and ac resistance at 50 ma dc. These tests were intended to serve as process checks and to weed out defective units before the coating process.

In addition to the above, 100 cells from each week's production were obtained, given identification numbers, and subjected to detailed spectral response tests; these cells were then antireflection coated and retested in detail. This permitted continued evaluation of the spectral behavior of the uncoated production cells, and of the improvement obtained by the coating process.

The test equipment for production line electrical tests used a slightly modified 35-mm slide projector as a light source. The heat absorbing glass filter in this projector cut off rather sharply in the near infrared; the resultant light was therefore "bluer" than sunlight at ground level. This test set was maintained by secondary standard cells which were calibrated in the laboratory spectral response set. As routine in-plant color tests were not made, the control of spectral response of the production cells was maintained indirectly — that is, by control of the diffused layer of the etched surface and of the antireflection layer later applied.

3.3.7 *Cell Antireflection Coating*

A single-layer interference antireflection film of SiO is vacuum evaporated onto the surface of the solar cell as the final step in its fabrication. SiO is generated by heating a mixture of pure Si and quartz (1:2 weight ratio, between 100 and 200 mesh) in a vertical tantalum tube

(0.157 inch ID, 2 inches long) pinched shut at the bottom and resistance heated. The solar cells are held by spring-loaded clips in a stainless steel dome of 13-inch radius, mounted 20 inches above the SiO source.

The film deposition is monitored by measuring the reduction in light reflection from a square of polished Si held in the center of the dome. A light source and blue-sensitive phototube pickup are mounted inside the vacuum chamber. A film about 800 Å thick is deposited in seven to ten minutes with a source heated to 1300°C and the vacuum at 5×10^{-6} torr or better. Deposition is stopped when the reflectance is a minimum for light between 0.50-μ and 0.55-μ wavelength.

The quality of the film is checked by suspending the coated cells for 30 minutes in steam over boiling water, and then visually inspecting them under diffuse light. Adherence of the film is tested by the simple Scotch Tape test. An acceptable coating shows no discoloration after steaming and none of it is stripped off by the Scotch Tape. Final electrical tests are relied upon to confirm the optical quality of the film.

3.4 Initial Performance of Completed Cells

Typical performance of production cells after antireflection coating is shown in Figs. 17 through 21, which summarize measurements on statistical samples from a group of more than 10,000 cells made in Sept., 1961. Fig. 17 shows the open-circuit voltage at 28°C. Although this is slightly lower than can be obtained with conventional p-on-n cells having a thicker diffused layer, the distribution of voltage values is consistent with a controlled process.

Fig. 18 shows the distribution of short-circuit currents and of cur-
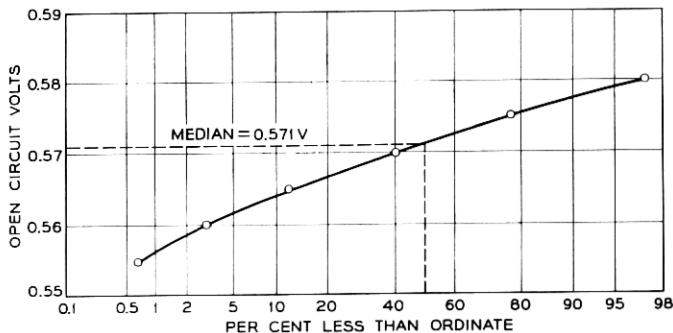

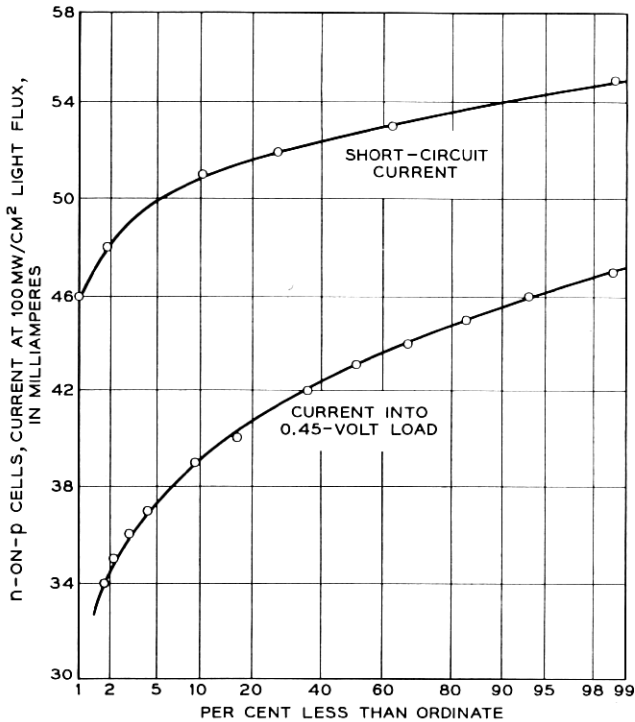Fig. 17 — Open-circuit voltage distribution.

Fig. 18 — Short-circuit current and current into 0.45-v load.

rents into an output load of 0.45 volt, made at an equivalent light flux of 100 mw/cm² sunlight. Fig. 19 shows the electrical conversion efficiency at a load voltage of 0.45 volts for 100 mw/cm² illumination with the light source described in Section 3.3.6. Fig. 20 shows a typical *V-I* curve and conversion efficiency versus load voltage. Fig. 21 shows typical improvement in current output, resulting from the SiO coating operation, versus incident wavelength.

3.5 *Selection of Cells for Module Assembly*

The range in cell current output into a 0.45-volt load (see Fig. 18) was from less than 36 ma to 47 ma. Advantages in performance would result if all cells of like current were grouped together or, more generally, if knowledge of the voltage, current, and temperature characteristics of the cells were used to optimize the performance of the solar cell modules and strings. As a practical operation, such optimization could
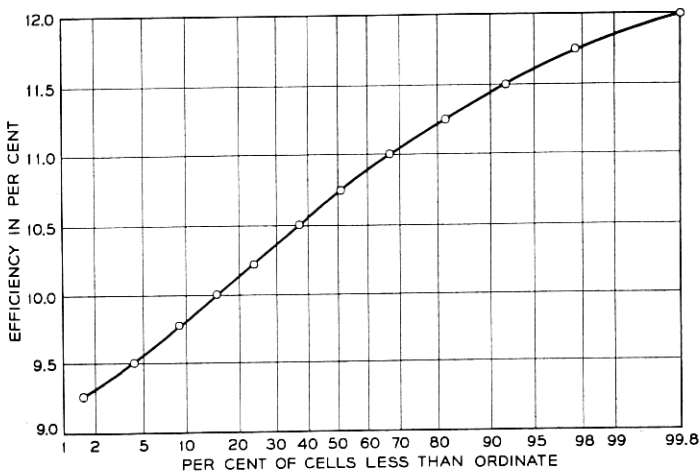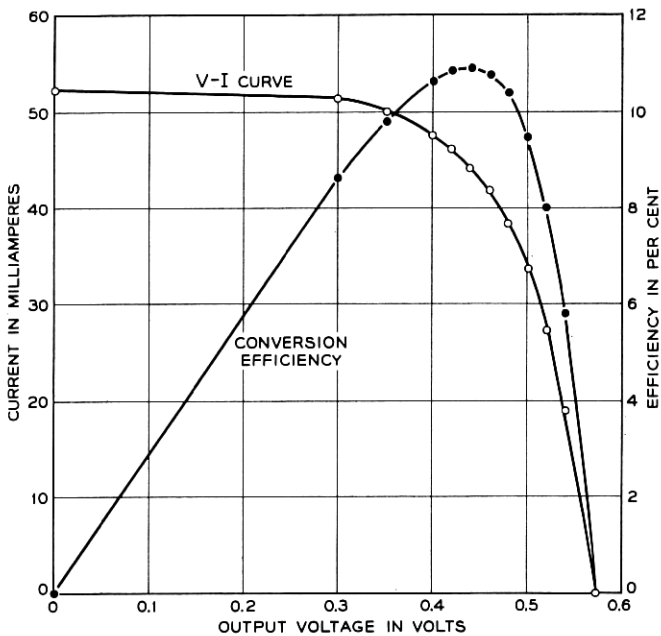
Fig. 19 — Conversion efficiency at 0.45 v.

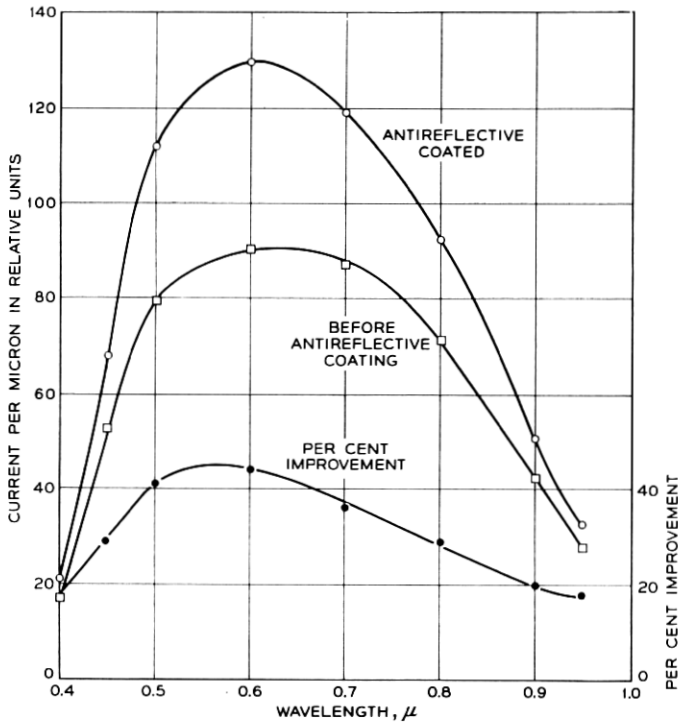Fig. 20 — Solar cell *V-I* and conversion efficiency vs load voltage.

Fig. 21 — Improvement in current response after application of antireflection coating.

only be approximated. To this end, the cells were sorted into groups; the current range for all cells in one group was held to 1 ma. For a particular 12-cell module, only cells from a particular group were used. Records were kept in such form that the performance of the completed module could be compared to that expected from the cells with which it was made. This information could be used to find modules in which serious changes or deterioration of cell performance resulted from the assembly operation. In most cases, however, there appeared to be little change in the cell performance when assembled into modules.

IV. MODULE DESIGN AND CONSTRUCTION

4.1 *Solar Cell Module Requirements*

The module must withstand two widely different environments: the launching environment, where it is subjected to extreme mechanical

vibration stresses; and the orbital environment, where it is subjected to radiation and cyclic thermal stresses. The following list of items is given as the primary design requirements for the module:

(1) provide radiation protection
(2) withstand thermal cycling stresses
(3) withstand vibration during launch and
(4) minimize temperature of cells.

The need for radiation protection has been discussed earlier in this paper. The protection should be provided on all sides of the cells. The protective material over the active surface of the cell must be transparent and not be affected by the radiation bombardment.

As the satellite assumes various attitudes with respect to the sun, surface temperatures vary from $+69°C$ to $-100°C$. These extremes might occur once or twice during the life of the satellite should the spin axis point toward the sun. The normal temperature range is $+10°C$ to $-50°C$ for full sunlight and maximum eclipse with the spin axis nearly perpendicular to the sun. The differential expansion of the materials induces stresses in the component parts of the module, when cycled over the stated temperature range. Continuous thermal cycling will eventually result in fatigue failures if the stress is not limited.

The modules are mounted on the external surfaces of the satellite and measurements show that, at resonances in the structure, accelerations in excess of 200 g's are present.

As the temperature increases, the conversion efficiency of the cells decreases, making it desirable to minimize the temperature of the cell. Considerations of temperature effects in the design of the solar plant are given in Section V.

4.2 *Design Objectives*

The design of the module can be divided into four main sections: the electrical design, the mechanical design, the thermal design and the radiation protection. These, of course, are all closely interwoven: for example, the mechanical design might dictate the expansivity of a material being chosen for a particular application, the thermal requirements limit the choice to a single material, and the radiation protection dictates the thickness of the material for minimum weight.

Electrically, the design must provide a series connection between the cells, insulate them from the satellite structure and provide terminals for interconnecting the modules.

The major mechanical objective is that the module withstand the vibration during launch. Fortunately, the mass of the module is small

so that even with accelerations of 200 g's the forces are small. Damping has been provided in the spring tabs that are used to fasten the modules to the panels.

It is important to minimize the temperature of the solar cells. The incident power not converted into electrical power must be removed from the cells and eventually reradiated into space. Direct reradiation through the sapphire covers is not possible, because a "greenhouse" situation exists: i.e., at the wavelength of the black-body radiation of the cell, the cover is opaque. Thus a thermally conducting path to the cover is required, and this should be of low thermal impedance. As the modules must withstand a wide range of temperature, coexpansive materials must be used.

Radiation protection is provided by enclosing the cells in a box structure consisting of the ceramic mounting plate, the transparent covers and a metal frame to join these two. The thickness of the material is obtained by dividing the required protection of 0.3 gm/cm² by the density of the material. Using this relationship, the thickness of the cover plates and ceramic is 30 mils and the thickness of the platinum frame is 8 mils.

4.3 Module Design

The solar cell module, shown in Fig. 22, is $4\frac{5}{8}$ inches long, $\frac{7}{8}$ inch wide, and $\frac{1}{8}$ inch thick, and weighs 0.8 ounce. It is made of two assemblies: the cover assembly, which consists of sapphire cover plates brazed into the platinum frame; and the solar cell assembly, which consists of the solar cells, shingled to provide a series connection, mounted on the ceramic plate. The two assemblies are joined by soldering the cover assembly to the cell assembly along the edges of the ceramic plate.

Several materials were considered for the transparent cover over the solar cells. Measurements of the transmission before and after exposure to radiation showed the suitability of certain glasses, quartz and sapphire. In weighing the other characteristics of the materials, sapphire was chosen for its higher thermal conductivity and the availability of processes for joining it to metals.

Table I shows some of the properties of the materials used in the module. As can be seen, the thermal conductivity of sapphire is 20 to 30 times greater than that of glass or quartz. Alumina ceramic, which is a polycrystalline form of sapphire, has approximately the same expansivity as sapphire. Platinum was chosen to join these together because it provides the closest expansion match and is nonmagnetic.

The selection of coexpansive materials limits the stress where these

SATELLITE SHELL

METHOD OF ANCHORING SOLAR CELL ASSEMBLY TO THE SATELLITE SHELL

SATELLITE SHELL

TAB

SOLAR CELL

ATTACHMENT OF SOLAR CELLS TO MOUNTING PLATE

METALLIZING

MICA

EPOXY

CERAMIC MOUNTING PLATE

MOUNTING SLOTS

MOUNTING PLATE ASSEMBLY

EXPANSION JOINT ASSEMBLY

COVER ASSEMBLY

INTERCONNECTING RIBBON

SOLAR CELL ASSEMBLY

CERAMIC MOUNTING PLATE

METHOD OF WIRING SOLAR CELLS

TABLE I — MATERIALS CONSIDERED FOR MODULE

Material	Expansivity, 10⁻⁶ in/in/°C	Thermal Conductivity, cgs Units
Silicon	2.4(20° C) −0.3(−173° C)	0.20
Sapphire	7.0	0.06
Fused quartz	0.5	0.003
Glass	10.0	0.002
Alumina ceramic	6.8	0.06
Platinum	8.0	0.16
Silver	19.0	1.06
Invar	0.5	0.03

materials are joined. The joints must have a low thermal impedance, since they are in the heat conduction path. A zirconium-silver active metal seal was developed for the joint between the sapphire and platinum.

Also shown in Table I is the expansivity of silicon. It should be noted that the expansivity decreases with temperature, reversing at a temperature of −180°C. Since no insulating material could be found which was coexpansive with the silicon, flexibility was provided by incorporating hinges or expansive joints between the cells and the ceramic. Silver is used for the expansion joints because of its ductility and good thermal conductivity. The conductance of the 1.5-mil silver expansion joint is the same as that of the 30-mil ceramic, since the coefficient of thermal conduction of silver is 20 times greater than that of the ceramic.

To compensate for the mismatch between the silver and the silicon, inserts of 0.001-inch thick Nilvar are used. When soldered between the silver and the silicon, the Nilvar retards the expansion of the silver and produces a joint capable of withstanding the thermal cycling.

4.4 Module Fabrication

4.4.1 Cover Assembly

The cover assembly is made by brazing 13 sapphire plates into a platinum frame with zirconium-silver. To minimize the gap between the covers, it is important that the long edges be parallel to and the short edges be perpendicular to them. Intimate contact for brazing was obtained by procuring the covers in sets matched within one mil in length.

The sapphire covers are brazed to the platinum frame in a fixture which maintains a planar surface for all covers and provides sufficient clamping pressure to insure intimate contact between the covers. The fixtures are placed in a retort which contains a purified nitrogen atmosphere and brazed at 975°C ± 10°C for 3 minutes. The temperature cycle during brazing is carefully controlled to minimize thermal shock.

4.4.2. *Antireflection Coating of Sapphire*

The polished sapphire covers placed over the solar cells to protect them from radiation damage transmit only 85 per cent to 87 per cent of the incident light. This loss, caused by surface reflection, reduces the solar cell output more than can be tolerated. An antireflection coating, therefore, is deposited on both sides of the sapphire cover assembly. The coating consists of a single-layer interference film of MgF_2 about 1000 Å thick. It increases the transmission to 90 per cent or more in the wavelength range from 0.4 μ to 1.0 μ, with a maximum transmission greater than 98 per cent between 0.5 μ and 0.6 μ. With this higher transmission, the covers reduce the solar cell module output by less than 5 per cent.

Micrometeorites will reduce the sapphire cover transmission by abrading the exposed surface. If this abrasion removes a 200 Å layer per year, as postulated by Jaffe and Rittenhouse,[14] the outer antireflection coating will be removed in three to four years, leading to a loss in initial cell output of about 6 per cent. Laboratory tests showed a 3 per cent loss in output for a mild abrasion of the antireflection-coated sapphire cover, and an 18 per cent loss for frosting of the sapphire. However, since the number and distribution of micrometeorites in space is not accurately known, a quantitative calculation of their effect on solar cell output cannot be made.

The antireflection coating is applied by evaporating MgF_2 from a hot, open tantalum boat in a vacuum of 9×10^{-5} torr or better. The boat is heated until the MgF_2 just melts, and the film is deposited in less than 3 minutes. The sapphire covers are held 20 inches above the boat on a stainless steel dome of 13-inch radius. Specially designed heaters are mounted on the dome so the sapphire covers can be kept at 300°C during the evaporation to assure a hard, adherent film. The film deposition is monitored by measuring the light reflected from one of the covers, using a blue-sensitive phototube as the pickup.

The quality of the antireflection film is checked by subjecting sample covers to 30 minutes in steam above boiling water in a covered vessel, then visually inspecting them. Transmission of the steamed covers is also measured at 0.4, 0.6, 0.8, and 1.0 μ.

4.4.3 *Mounting Plate Assembly*

The solar cell mounting plate consists of the solar cells, the expansion joints, the ceramic mounting plate and the electrical leads from the cells to the terminals.

The solar cells are delivered in matched sets as previously described. The expansion joint, which consists of a folded silver sheet with two narrow strips of Nilvar soldered to one edge and a mica sheet inserted in the fold, is soldered to the back edge of each cell. The mica insert prevents the solder from joining the flaps of the fold, which would spoil the flexibility of the expansion joint.

The cells are assembled in a fixture with the ceramic mounting plate for the soldering operation. The ceramic plates have metallized areas which are located to join the free end of the cell expansion joint. Prior to assembly in the fixture, the metallized areas are silver plated and coated with solder. Other metallized areas are provided on the ceramic that serve as the terminals and joining surfaces for the cover assembly. Individual weights on the cells force the expansion joints into contact with the ceramic. The fixtures are placed in a retort with a nitrogen atmosphere and heated to flow the solder. The nitrogen atmosphere is used in all soldering operations in lieu of organic fluxes. After removal from the fixture, the leads are connected to the terminals and the assembly is tested for continuity.

4.4.4 *Module Assembly and Test*

The two assemblies are soldered together at the joint between the platinum frame and the edge of the ceramic. This is done in a fixture in which pneumatic cylinders press electrically heated pads against the platinum frame and force it into contact with the ceramic plate. The temperature of the pads is controlled by thermocouples, and the soldering cycle is controlled by a timer.

The completed modules are evaluated mechanically, electrically and thermally. The mechanical test consists of a microscopic inspection which eliminates any obvious mechanical flaws such as cracked cells, incomplete solder joints or poor alignment of cells on their mounting plates. Because of the fragility of the cells and the inaccessibility of some solder joints for microscopic inspection, two stressing tests are used. The first of these tests is a vibration test during which the module is vibrated for 30 seconds at 20 g's at 600 cps. The second test is a thermal cycling test, in which the modules are cycled from $+65°C$ to $-100°C$ for a total of 6 cycles. The stresses induced by these tests eliminate the manufacturing freaks. The electrical tests are measurements of the electrical output of the module under a controlled illumination. The results of these tests are used for grouping the modules into different classes, and will be discussed in detail later.

4.5 *Module Mounting*

Each module is equipped with six beryllium-copper twist tabs for mounting. These tabs are inserted in slots in the reinforced aluminum panels. A molybdenum strip, with matching slots, is placed in back of the panel with the tabs projecting through the slots. The tabs are twisted a quarter turn, which causes slit ends to emerge from the slots and to form spring fingers which hold the module in contact with the panel.

Six modules are connected in series to form a string which provides the required 28 volts. Omega loops made of braided copper wire are soldered to adjacent terminals to connect the modules in series. The end terminals in the string are connected to glass seal terminals mounted in the panel. Two additional terminals are provided for each string of cells and are positioned approximately $\frac{3}{4}$ inch above the string terminals. A blocking diode is connected between the string terminal and the adjacent added terminal. A connection is provided between the upper terminals, so that the output of a string appears at one side of the panel. This arrangement has the advantage that all current paths are brought back upon themselves, so that no retarding torques due to current loops in the solar cell wiring are applied to the satellite. The same precautions are taken in the internal wiring harness that connects the solar cell plant to the electronics chassis.

4.6 *Solar Cell Module Testing*

Fig. 23 shows the expected temperature ranges on the surface of the satellite with the sun perpendicular (pos. 1) and parallel (pos. 2) to the spin axis. Thermal test ranges and test results are also given.

The slow cycling tests were conducted in an oven-refrigerator combination in which the maximum rate of change of temperature was 3°C/min. The temperature was varied from +65°C to −100°C. This rate of change was faster than the expected 2°C/minute in space, and the temperature excursion was greater than the 40° range expected for any module under orbital conditions. The results are indicated on the graph. After 800 cycles, 3 modules had failed, with the failures occurring at 300, 675 and 800 cycles. The failures were at solder joints.

For the thermal-vacuum tests, modules were sealed in evacuated glass vials. These were mounted on a sun-seeking servo system which maintained the surface of the module perpendicular to the sun. Maximum and minimum temperatures of +60°C and −10°C were observed. Twelve modules have been on test over a year with electrical checks at
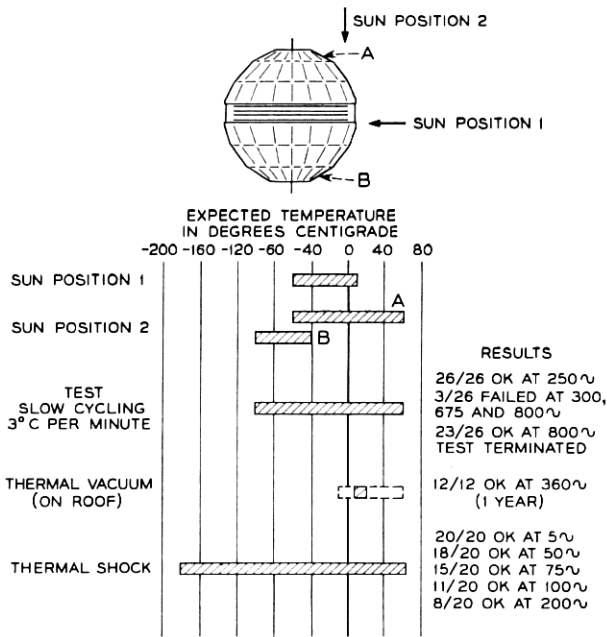
Fig. 23 — Expected satellite skin temperature for two conditions of illumination.

3-month intervals. There have been no significant changes in the modules on test.

For thermal shock tests, modules were sealed in polyethylene containers to prevent condensation. They were then heated and stabilized at 65°C in an oven. They were removed and immediately plunged into liquid nitrogen and held there until the temperature stabilized. The procedure was then repeated. After 200 cycles, 8 of the 20 modules were still operable. In all cases the failures occurred at the soft solder joints to the solar cells.

During early development, vibration tests were made on individual modules, using levels of 100 g's. These tests were all successful. However, it was not until a frame and panels were available that the transmissibility of the structure was known. A complete complement of 300 modules was mounted on the mechanical model satellite. Table II shows the tests to which the cells mounted on the satellite were subjected. Peak accelerations of 200 g's were measured. The failures that occurred at the fifth-resonance dwell test were all at solder joints. These

TABLE II — VIBRATION TESTS ON 300 MODULES MOUNTED
ON MECHANICAL MODEL SATELLITE

Test	Number of Tests	Module Condition
Qualification level in thrust direction	5	ok
Resonance dwell	4	ok
Resonance dwell	fifth test	6/300 modules failed at soft solder joints

failures were due to fatigue of the solder, which had been subjected to 750,000 cycles at the time of failure.

The foregoing tests were in essence qualification tests of the module. During production of the module it was necessary to detect any modules that would not withstand the thermal or vibration environment. All modules were therefore subjected to two environmental tests: a thermal cycling test and a moderate-level vibration test. The purpose of these tests was to subject the module to cyclic stresses that would cause weak joints to fail.

The thermal test consisted of cycling the modules from $+65°C$ to $-100°C$ at a maximum rate of change of $3°C/min$ for a total of 6 cycles. The modules were evaluated by a microscopic inspection and electrical tests. Ninety-five per cent of the modules subjected to this test were later found acceptable.

All modules were vibrated at 600 cps for 30 seconds at an acceleration of 20 g's. Again, 95 per cent of the modules were acceptable, based on microscopic inspection and electrical tests.

V. SOLAR PLANT DESIGN AND PERFORMANCE

5.1 *General Design Considerations*

The integration of individual solar cells or of modules into a solar plant depends on several variables with strong interactions and possible trade-offs between them. The key variables are satellite shape and available surface area, operating temperature, satellite orientation in space, and required average output if chemical batteries are used, or required minimum output otherwise.

The Telstar spacecraft is a spherical, spin-stabilized satellite with solar cells attached to its surface. For such a solar plant the most favorable orientation is one where the spin axis and the sun-satellite line form an angle of 90°, i.e., equatorial illumination of the satellite. Such an

orientation of a spinning satellite will result in the lowest solar plant operating temperature. In the absence of perturbations, the satellite orientation will remain constant. However, interactions of the earth's magnetic field with any residual magnetic moment of the satellite cause precessions of the spin axis. Although ground commandable torquing coils are provided on the spacecraft for controlling such spin-axis precession, it was required for reasons of over-all reliability that the solar plant give usable power for any orientation. The design problem was thus to find the best distribution of the cells on the surface that would do this. Since the output current of series-connected cells is governed by the cell having the lowest output, all cells in a series string should have matched characteristics and should be mounted in one plane so as to receive the sunlight under the same angle of incidence. Thus, while electrically such a group of cells represents a string, in their geometrical layout they form a block or a patch.

If the temperature of the skin were uniform under all conditions, then the design objective would be achieved by distributing solar patches uniformly over the surface. However, since thermal conduction along the skin of the satellite is negligible, temperatures are established predominantly by radiative energy exchanges; therefore, the region facing the sun gets hottest. Under equatorial illumination, a given region near the satellite's equator receives sunlight at near normal incidence only a fraction of the time. Half of the time it is in the shade facing away from the sun. Thus, the average temperature on the equatorial band is low (1°C) and that of the poles is even lower (−3°C). Since the satellite's period of revolution is small compared to the thermal time constants, the instantaneous temperatures deviate little from the average temperature. Under polar illumination, however, one polar region faces the sun all the time and gets hot (+69°C) while the other gets very cold (−100°C). As the solar cell output in the voltage range of interest decreases with increasing temperature, the output under polar illumination would be lowest and that under equatorial illumination highest if solar patches of equal output characteristics were distributed evenly over the sphere. Some equalization is needed; it can be achieved by selective placement of high-output patches, and by increasing the patch density in the polar regions.

The output of the solar plant is connected directly across the batteries and the input regulator. The battery voltage, and thus the voltage into which the solar plant delivers its current, varies under normal operation between 25 and 28 volts, depending on the power demand schedule. One is thus interested, not in the solar plant current at a fixed voltage

only, but rather in the current-voltage output characteristic of the solar plant. Knowing the current-voltage characteristic of the individual cells as functions of temperature and angle of sunlight incidence, and knowing the temperatures of the solar patches for a given geometrical patch distribution and a given solar aspect (i.e., angle between sun-satellite direction and spin axis), the solar plant output characteristic can be calculated. While simple in principle, such calculations are quite lengthy and are most conveniently done on an electronic computer. The details of these calculations are presented in Section 5.5, and computed output curves representing the final design are shown in Figs. 28 and 29 of that section.

Finally, since the Telstar satellite operates with chemical storage batteries, it is the average output power which must satisfy the minimum output requirement, and not the instantaneous output power. Thus, the distribution of the solar cells need not be uniform over the entire surface — only the distribution averaged over one satellite rotation need be considered.

5.2 *Solar Plant Size and Configuration*

Since it is known that the output of the solar plant will decrease with time because of radiation damage, the most efficient use of this reduced output will be obtained if the solar plant delivers its maximum end-of-life power at the terminal voltage of the power plant when the batteries are being charged. Radiation damage studies have shown that a solar cell of the type used delivers its maximum power at approximately 0.4 volt after damage corresponding to about two years in orbit.[15] Since the terminal voltage of the power plant is roughly 28 volts when the batteries are being charged, strings of 72 series-connected solar cells were chosen to be the basic building blocks for the solar plant.

Considerations for the distribution of the patches were given above. One variable, however, has not been discussed yet, and that is the ratio of solar cell area to total satellite surface area. At places where there are no solar cells, the skin is covered with a material (aluminum oxide) which is highly reflective to or has a low absorptivity for sunlight in the 0.4-μ to 1.5-μ wavelength range containing most of the sunlight's power, but which is highly emissive at long wavelengths corresponding to the black body radiation at the temperature of the satellite. The ratio α/ϵ of the absorptivity at short wavelengths to the emissivity at long wavelengths is ≈ 0.22 for aluminum oxide and 1.7 for the solar cell

patches. Thus the larger the coverage with solar cells is, the higher will temperatures be. Since the canister is in radiative temperature equilibrium with the skin, its temperature is governed by the average skin temperature. For reliability reasons, a canister temperature near room temperature is highly desirable. Thus the canister temperature provided a strong constraint in decisions concerning the solar cell coverage. Another constraint was the weight per unit power. With higher coverage, a larger power output can be obtained on a sphere of given diameter. However, since the cells are then hotter, they work with lower efficiency, and the solar cell weight per watt goes up.

In the final design 50 parallel strings are used, incorporating a total of 3600 cells. This provides an initial power of about 14 watts and allows for an average of about 3.5 hours of transmission time per day — a reasonable figure, since the time of mutual visibility between Andover and Europe is about four hours when apogee is in its most favorable position. The distribution of cells on the surface is shown in Fig. 24.

5.3 Selection and Placement of Modules

The assembled modules were tested under a light source which provided uniform illumination over the 12-cell area of an intensity equivalent to 100 mw/cm^2 of solar illumination. The short-circuit current and the current at 5.4 volts (an average voltage of 450 mv per cell) were measured and recorded, and those modules having lower output than 38 ma at 5.4 volts were rejected for satellite use. The accepted modules were grouped into six-module strings by selection of modules which had matched short-circuit currents and currents at 5.4 volts under the test conditions. If there were insufficient modules having matched output currents to form a string, modules having higher current output under either or both test conditions were used to complete the string.

The six-module strings having the highest output currents were located on the bands nearest the poles of the satellite. This was done to provide the maximum output possible under the most unfavorable condition of illumination, namely, that of the spin axis of the satellite pointing toward the sun. The strings having the least output (of those selected for solar plant use) were located on the bands nearest the equator of the satellite, since cells on these bands operate at the lowest temperature.

Fig. 25 shows the distribution of currents at 5.4 volts obtained for 345 assembled modules at an equivalent light intensity of 100 mw/cm^2.
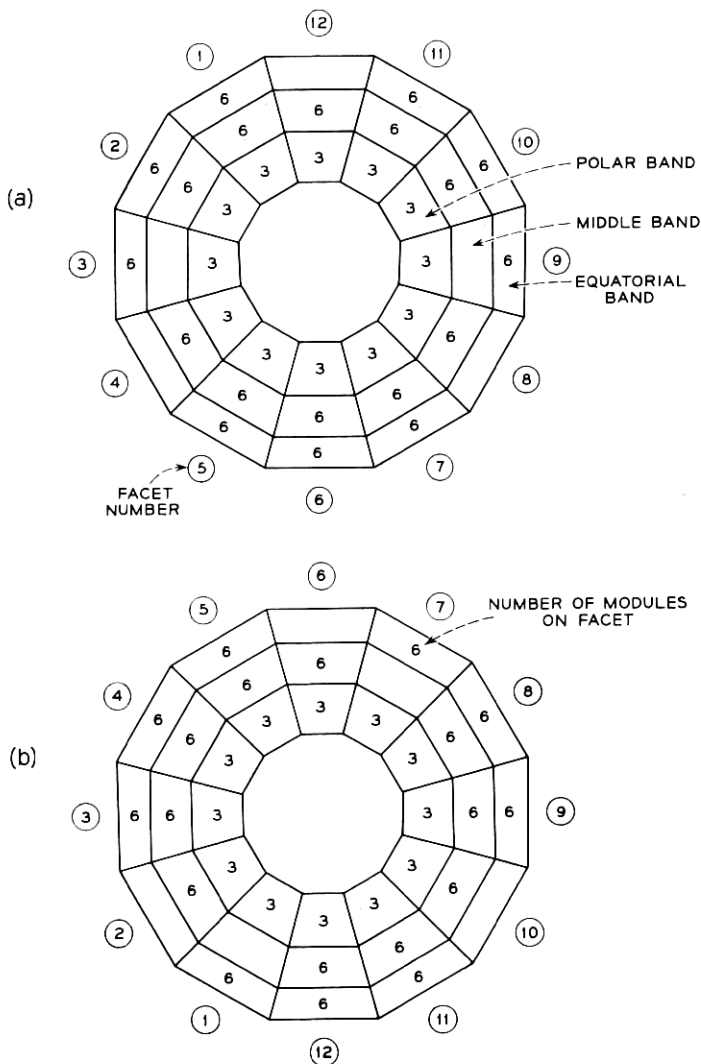
Fig. 24 — Distribution of solar cell modules on surface of Telstar spacecraft.

5.4 *Blocking Diodes*

The solar cell strings cannot be connected in parallel directly, since the dark cells would constitute a current drain. Instead, the positive terminals of all the strings are connected to the output bus by rectifier diodes. These diodes present a low impedance to the output current of
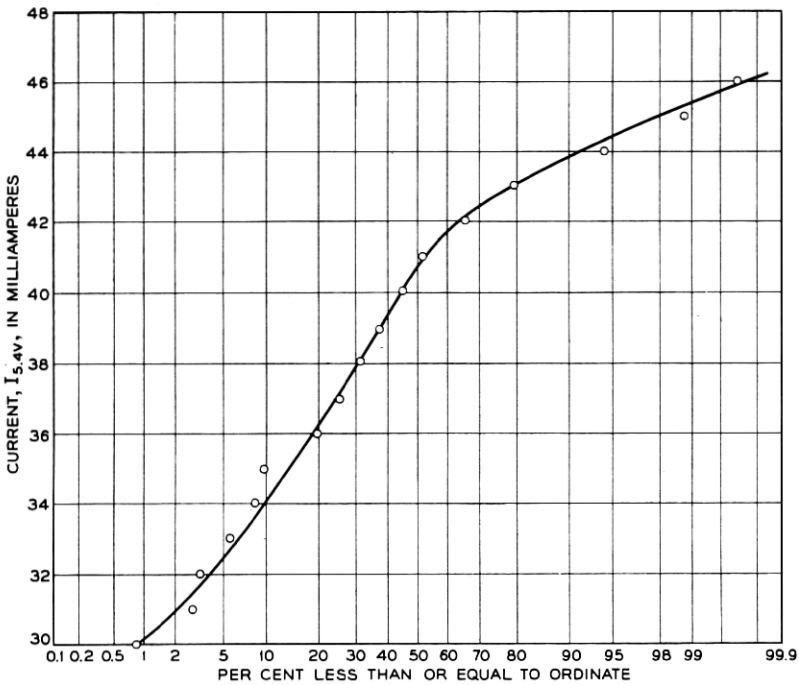
Fig. 25 — Module output current at 5.4 v.

illuminated strings, while their high reverse impedance prevents current leakage through dark cells. The rectifier diodes also prevent discharge of the batteries if a short from any portion of a string to the frame should develop, as might be the case under micrometeorite impact.

5.5 Solar Plant Output Characteristic

In the Telstar program, inspections and performance checks after each assembly step were undertaken whenever possible. The testing of the individual solar cells and of the modules was described above. However, adequate tests under simulated space environment of the completed solar plant on the satellite shell were not feasible. While thermal tests were made when the satellite was in a space-simulation chamber, the uniformity and collimation of the light source (3 carbon arc lamps) were insufficient to allow precision measurements of the expected outer space performance, and calculations had to be relied on. Such calculations were also important during the design phase, when the various trade-offs

were explored. These calculations were initially done by hand, but were later programmed for an IBM 7090 computer. We shall sketch below how the input information was obtained and present the important results of the calculations.

For convenience, all strings on a given band were considered to consist of 72 identical series-connected cells having characteristics representative of the cells used on the band. The output characteristic of a cell on the satellite shell depends on the angle of incidence and on temperature. In measuring cell characteristics, it was convenient to introduce the short-circuit current as an intermediate variable. One thus needed the output characteristic as a function of short-circuit current and temperature, and the short-circuit current as a function of angle. Simple geometrical reasoning would lead one to expect a cosine-law dependence for the latter; actually, however, between the incident light and the solar cell there is the antireflection coating of the solar cell and the sapphire cover with antireflection coatings on either side. Thus, a more complicated angular dependence results.

To determine the combined effect of these factors, as well as the effect of any shading or reflections caused by the module structure at near glancing angles of incidence, measurements were made of the short-circuit current output of sapphire-covered solar cells as a function of the angle of illumination using terrestrial sunlight. For these measurements, a baffle tube having a 0.1-radian acceptance angle was used to eliminate sky radiation, and the cells were mounted on a temperature-controlled base which could be rotated. Measurements were made at temperatures ranging from $-70°C$ to $+65°C$ on unbombarded cells and on cells bombarded with 2×10^{16} 1-Mev electrons/cm². The relative variation of short-circuit output current with the angle of illumination was found to be independent of both temperature and bombardment level. A normalized plot of this variation is shown in Fig. 26.

A typical output characteristic for short-circuit currents of 25 and 50 ma and temperatures of $-20°$ and $+40°C$ is shown in Fig. 27. To the first order, a change in short-circuit current corresponds to a shift of the characteristic parallel to the current axis. Second-order changes result from the front layer sheet resistance and contact resistance. To obtain the characteristic as a function of short-circuit current and temperature, precision measurements were made of the characteristic of a median cell at a set of 13 short-circuit currents and 6 temperatures. These are stored in the computer program, so that by interpolating between them reliable characteristics can be obtained for any short-circuit current and temperature required in the calculations.

Using the input data just described, the initial current and power out-
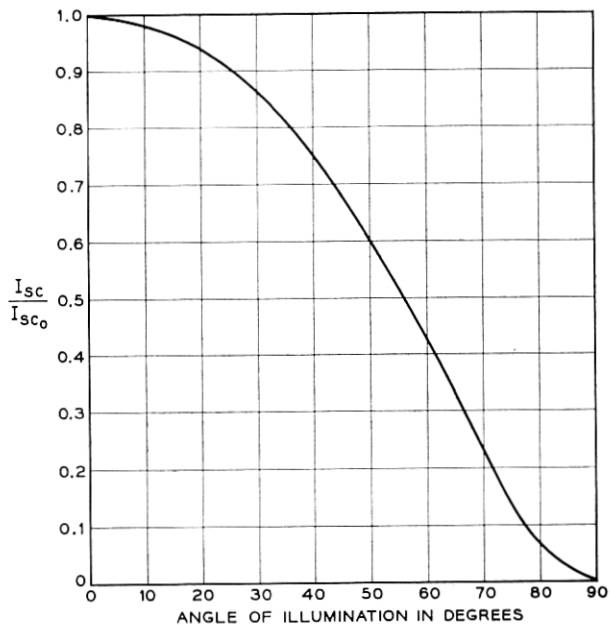
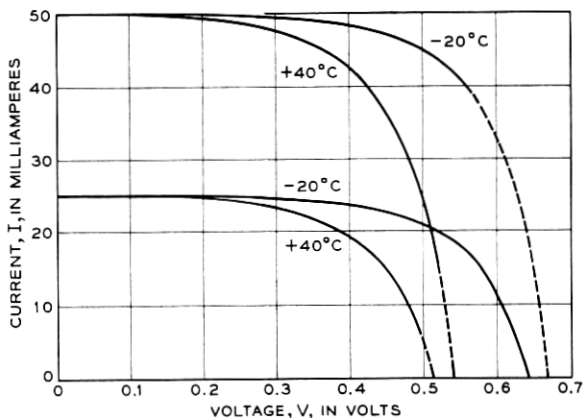Fig. 26 — Normalized short-circuit current vs angle of illumination.

Fig. 27 — Typical solar cell output characteristic.

put characteristics of the spacecraft solar plant for four conditions of illumination were calculated and are shown in Figs. 28 and 29. The angles which identify each curve in these figures define the aspect angle between the spin axis of the satellite and the satellite-sun line. The time-
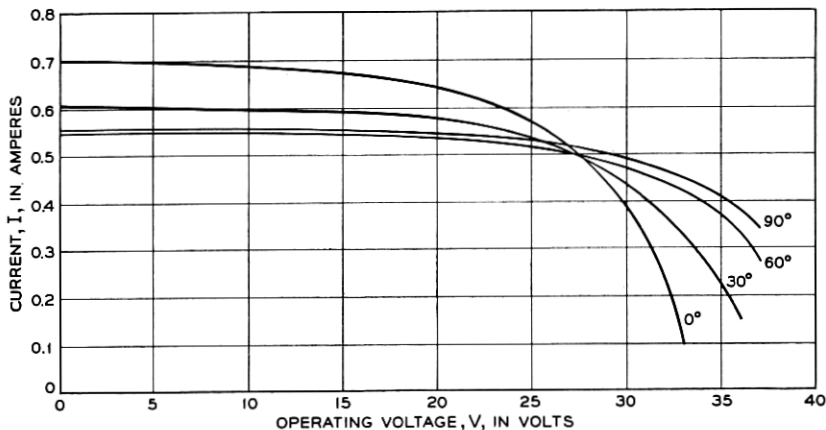
Fig. 28 — Calculated initial current output characteristic of the spacecraft solar plant.
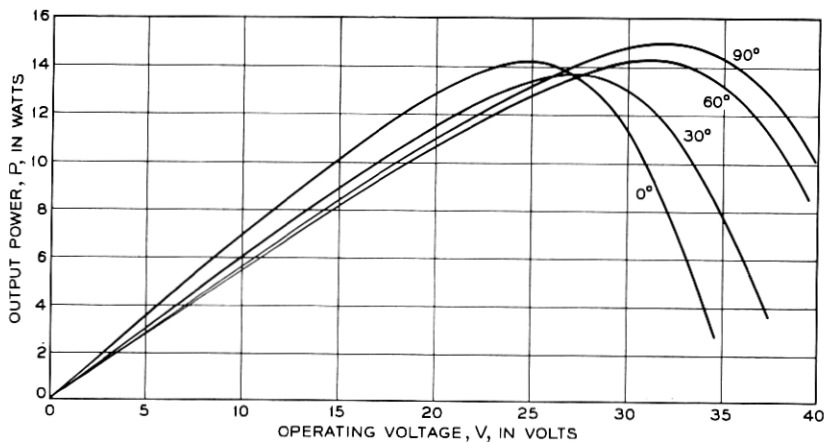

Fig. 29 — Calculated initial power output characteristic of the solar plant.

averaged output current contributed by each band was computed as a function of the operating voltage, taking into account the aspect angle, the calculated operating temperature of the cells on the band, the angle between the normal to the band and the spin axis, the efficiency of the strings and the number of strings on the band. The average solar plant output current is then the sum of the individual band outputs. The variation in the output characteristic with aspect angle is due primarily to the increased operating temperature of the solar cells as the aspect

TABLE III—CALCULATED BAND TEMPERATURES AS A
FUNCTION OF ASPECT ANGLE

Band	Aspect Angle			
	0°	30°	60°	90°
1	69°C	49°C	15°C	−3°C
2	63°C	44°C	25°C	8°C
3	13°C	8°C	8°C	1°C
4		−70°C	−34°C	1°C
5			−41°C	8°C
6			−69°C	−3°C

angle changes from 90° to 0° as shown in Table III.[16] The increased short-circuit current at an aspect angle of 0° is the result of locating modules of a greater short-circuit current output near the poles of the satellite, as described earlier. The more rapid decrease of output current with increasing voltage at this aspect angle is entirely due to the high operating temperature of the modules. The solar plant was designed so that these two effects tend to compensate, and thus the initial output current at the battery charging voltage of about 28 volts is nearly constant, regardless of the orientation of the satellite in space.

5.6 Flight Performance of the Solar Plant

The first average current output from the Telstar solar plant after launch was obtained from telemetry data taken during pass 6. The average current during this pass was 492 ma at an average solar plant operating voltage of 24.8 volts. At the time of launch, the solar intensity was approximately 3.3 per cent less than mean solar intensity. Therefore, at mean solar intensity the output current would have been 509 ma for the same operating voltage. This is to be compared with the computed initial output current of 530 ma at 24.8 volts as shown in Fig. 28.

Immediately prior to launch it was discovered that one solar cell module in each of two strings had developed an open circuit due to thermally induced stresses during preflight testing. Since time did not permit replacement of these defective modules, they were electrically bypassed. Thus, two of the 50 strings of solar cells on the Telstar satellite are operating with only 60 series cells. Since near the operating point the output current varies only slowly with voltage, this defect has resulted in a loss of only about 0.2 per cent in average output current.

The average solar plant current for the first 160 days of operation is plotted as circles in Fig. 30. A number of corrections were applied in
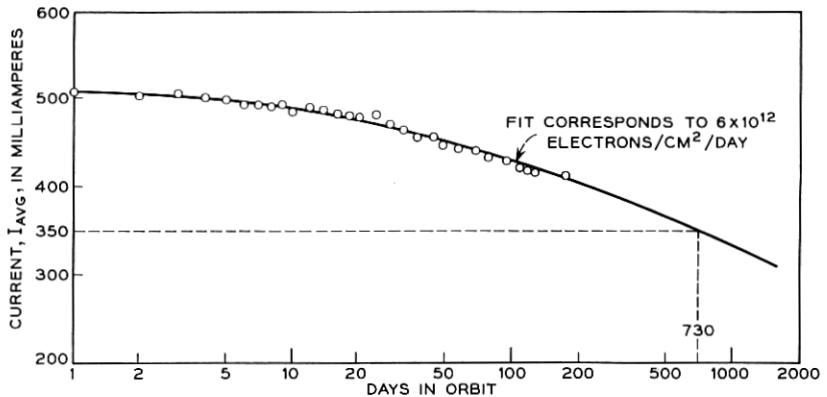
Fig. 30 — Average solar plant output current vs time in orbit.

Fig. 30 in order to suppress variations in output current that are not caused by radiation damage. The output current shows a peak-to-peak ripple of approximately 15 per cent. This ripple profile is scanned at a varying strobe rate as the spin rate changes. Care was taken to obtain a representative sample of the profile when extracting an average current. The variation due to solar distance changes was eliminated by normalizing to mean solar distance. The effect of changing load voltage was minimized by using only the measurements taken when the battery was near 25 volts. Corrections for temperature variations and variations in solar aspect were not applied. Thus the data in Fig. 30 must be considered preliminary; it is expected that the influence of the neglected corrections is small, but that their application may reduce the scatter in the points.

If the Telstar satellite had been exposed to a time-invariant radiation environment, then it should be possible to fit the observed output current points of Fig. 30 to a degradation curve under 1-Mev electrons similar to Fig. 4 by using a proper scale factor to convert time into 1-Mev electron flux. Fig. 4 shows the degradation of the short-circuit current of an average single cell; what is needed here is a corresponding curve for the output current of the solar plant at standard conditions (voltage, temperatures, solar aspect). Such a curve was computed, using the 1-Mev electron bombardment results of Section II, and is shown as the solid curve in Fig. 30. The ordinate scale was adjusted so that the initial value coincides with the measured one. The conversion factor for the abscissa which gives the best fit is 6×10^{12} electrons/cm^2 per day. Thus, the average radiation environment at the surface of the solar cell (i.e.,
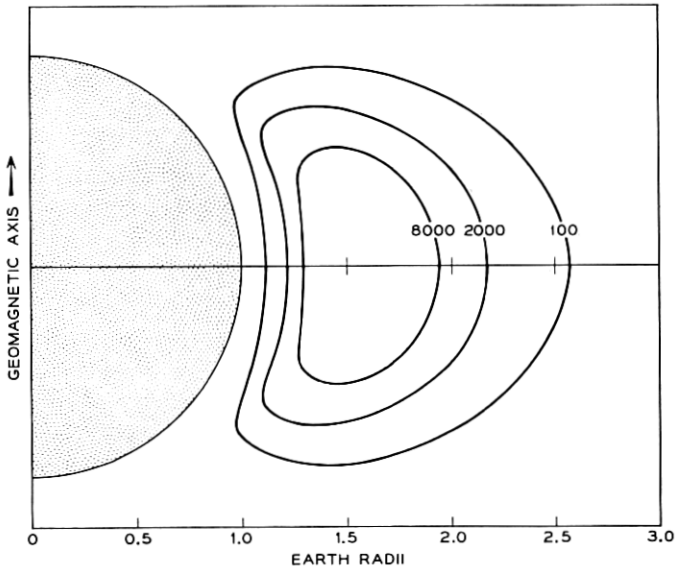
Fig. 31 — Isointensity contours of omnidirectional 24–36 Mev flux in protons/ cm² per second.

behind the sapphire) can be characterized as being equivalent to a normal-incidence 1-Mev flux of 6×10^{12} electrons/cm² per day. We shall now compare this number with recently measured particle fluxes.

The satellite carries three proton counters, which cover the energy range of 3.5 to 80 Mev in three noncontiguous channels. Analysis of the counter data is only preliminary, and absolute flux values are of limited accuracy because of uncertainties in counter calibrations. The data of the counter whose sensitivity is in the 24 to 36 Mev range yield isointensity contours of omnidirectional flux as shown in Fig. 31 in equivalent dipole coordinates. Satellite perigee and apogee are at 1.15 and 1.9 earth radii, respectively, in geocentric coordinates, and are variable by about ±0.1 earth radius in dipole coordinates because of the magnetic irregularity of the earth. Measurements within the highest contour are not sufficiently extensive to allow the plotting of another contour, but they do indicate the existence of flux values three times as high as shown. Fluxes of this magnitude are not sufficient to account for the radiation damage observed in Telstar. More recent proton measurements on Explorer XV indicate fluxes of three orders of magnitude greater than the above for the energy range 4 to 12 Mev.[17] It thus appears reasonable that protons of energies greater than 14 Mev, which includes those protons able to penetrate the 30 mils of sapphire shielding, occur in

sufficiently high fluxes to produce an appreciable portion of the observed damage to the solar plant.

The electron counter on the satellite was designed to measure efficiently electrons of energy below 1 Mev.[18] The pulses are sorted into four channels, covering an energy-event range of 180 Kev to 990 Kev. The depletion layer width of the counter is such that electrons of energies between 200 Kev and 600 Kev are counted with relatively good efficiency as compared to those of higher energies. Thus, if the counter is operated in a radiation environment containing relatively high intensities of multi-Mev electrons, it is possible to get flux values only by making assumptions concerning their energy distribution. In arriving at the average electron flux to which the Telstar solar plant has been exposed, it has been assumed that in the high-intensity regions of the radiation belt the energy distribution is that of a uranium fission electron spectrum.[19] Under this assumption, the average intensity for the four-month interval from July to October, 1962, of the omnidirectional flux is found to be about 10^8 cm^{-2} sec^{-1}, for electrons of all energies.*

Time variation of the electron intensity arises from two causes: (1) a decay in intensity at a fixed position in space, the decay rate factor varying with position, and (2) a variation due to the precession of perigee. Both of these factors were estimated from the variation of counting rate in the third highest energy channel and were used in evaluating the July through October time average flux.

Preliminary experiments on the damage rates for multi-Mev electrons as a function of energy and absorber thickness indicate that a fission spectrum flux of omnidirectional intensity of 10^8 cm^{-2} sec^{-1} corresponds to an equivalent 1-Mev electron flux (normal incidence on an unshielded cell) of about 3×10^{12} cm^{-2} day^{-1}.

On the basis of the calculated equivalent electron flux of 3×10^{12} cm^{-2} day^{-1} for the radiation belt electron contribution to the solar plant degradation as compared to the observed 6×10^{12} cm^{-2} day^{-1} equivalent flux, it now appears that multi-Mev electrons are responsible for about half the observed damage, and protons are responsible for the remainder. A detailed comparison of the equivalent 1-Mev flux damage with the measured proton and electron fluxes is given in Ref. 20.

VI. SUMMARY AND CONCLUSIONS

Analysis of environmental effects on the performance of medium-altitude communication satellites showed that a severe radiation dam-

---

* Recent electron counter measurements on Explorer XV indicate that the average multi-Mev electron intensity may have been overestimated by about a factor of two.[17]

age problem exists. However, a useful power plant life on the order of years can be obtained by use of solar cells designed for high radiation resistance and by shielding of the solar cells.

Radiation resistance of silicon solar cells in space is achieved by designing them to be highly responsive to short-wave photons near the solar peak, by using the n-on-p structure, and by minimizing all losses which are not radiation-damage dependent. These include reflection losses, series and shunt resistive losses, and surface recombination losses. Special attention was given to development of a low-resistance electrical contact with good adherence to polished silicon surfaces.

The cells are mounted in 12-cell modules designed to be resistant to thermal shock and cycling, to provide a minimum of 0.3 gm/cm² protective shielding, and to withstand acceleration and vibration stresses encountered in launching. Inorganic materials are used in the module assembly to avoid deterioration in the space environment. Fifty strings of six modules each are connected in parallel to provide a nominal 28-volt output of 14 watts. The strings are mounted on the satellite skin in a configuration which provides substantially constant output for any orientation of the spin axis relative to the sun-satellite line.

The Telstar spacecraft solar plant output, as obtained from telemetry data, decreases with time as a result of particle irradiation. The time dependence agrees with that of an unbombarded solar cell that is exposed in the laboratory to a 1-Mev electron flux of 6×10^{12} electrons/ (cm² day). From this comparison it is estimated that the plant will degrade to 68 per cent of its initial value after two years in orbit. Without other failures, occasional operation of the video channel should be possible even after 20 years in orbit, when the charging current will be in the order of one-half the initial value.

In future communication satellites, where switching is not used, the extension of solar power plant life to many years will be feasible by increasing the number of cells over that required initially. The penalty is not particularly severe, however, because of the logarithmic dependence of output on integrated radiation flux. For example, to extend the life of a particular power plant from two years to 20 years would require only about 20 per cent more cells on the satellite.

VII. ACKNOWLEDGMENT

REFERENCES

1. Chapin, D. M., Fuller, C. S., and Pearson, G. L., A New Silicon p-n Junction Photocell for Converting Solar Radiation into Electrical Power, J. Appl. Phys., **25**, Jan., 1954, p. 676.
2. Smith, D. H., A 1-Watt Solar Power Plant, Communications and Electronics, No. 54, November, 1959.
3. Van Allen, J. A., Geomagnetically-Trapped Corpuscular Radiation, J. Geophys. Res., **64**, Nov., 1959, pp. 1683–1689.
4. Loferski, J. J., Rappaport, P., and Scott-Monck, J., Radiation Damage to Silicon Solar Energy Converters, R.C.A. Labs Quarterly Report No. 1, NASA Contract NAS5-47, October 15, 1960.
   Mandelkorn, J., Kesperis, J., McAfee, R., and Pharo, W., A New Radiation Resistant High Efficiency Solar Cell, NASA meeting on Radiation Damage to Semiconductors by High Energy Protons, Washington, D. C., October 20, 1960.
5. Naugle, J. E., and Kniffen, D. A., Flux and Energy Spectra of Protons in the Inner Van Allen Belt, Phys. Rev. L., **7**, July, 1961, pp. 3–6.
6. Freden, S. C., and White, R. S., Particle Fluxes in the Inner Radiation Belt, J. Geophys. Res., **65**, May, 1960, pp. 1377–1383.
7. Conference on Radiation Effects in Semiconductors, J. Appl. Phys., **30**, May, 1959.
8. Gummel, H. K., Smits. F. M., and Froiland, A. R., Method for Terrestrial Determination of Solar Cell Short Circuit Current under Outer Space Solar Illumination, I. R. E. WESCON Proc., July, 1961.
9. Gummel, H. K., and Smits, F. M., to be published.
10. Rosenzweig, W., Diffusion Length Measurement by Means of Ionizing Radiation, B.S.T.J., **41**, Sept., 1962, pp. 1573–1588.
11. Rosenzweig, W., Gummel, H. K., and Smits, F. M., Solar Cell Degradation under 1-Mev Electron Bombardment, B.S.T.J., **42**, Mar., 1963, pp. 399–414.
12. Rosenzweig, W., Smits, F. M., and Brown, W. L., Nuclear Electronic Effects Program, Tenth Triannual Note, July 15, 1962.
13. Naugle, J. E., and Fichtel, C. E., Flux and Energy Spectra of Protons in the Inner Van Allen Belt, Am. Phys. Soc. Bulletin II, **6**, Feb., 1961, p. 53.
14. Jaffe, L. D., and Rittenhouse, J. B., Behavior of Materials in Space Environment, Am. Roc. Soc., Meeting, Oct. 9–15, 1961.
15. Smits, F. M., Smith, K. D., and Brown, W. L., Solar Cells for Communication Satellites in the Van Allen Belt, J. Brit. Inst. Radio Eng., **22**, Aug., 1961, pp. 161–169.
16. Hrycak, P., Koontz, D. E., Maggs, C., Stafford, J. W., Unger, B. A., and Wittenberg, A. M., The Spacecraft Structure and Thermal Design Considerations, B.S.T.J., this issue, p. 973.
17. Brown, W. L., private communication.
18. Brown, W. L., and Gabbe, J. D., Electron Distribution in the Earth's Radiation Belts during July, 1962, as Measured by Telstar, J. Geophys. Res., **68**, Feb. 1, 1963, p. 607.
19. Carter, R. E., Reines, F., Wagner, J. J., and Wyman, M. E., Expected Cross Section from Measurements of Fusion Fragment Electron Spectrum, Phys. Rev., **113**, Jan., 1959, pp. 280–286.
20. Brown, W. L., Gabbe, J., and Rosenzweig, W., Results of the *Telstar* Radiation Experiments, B.S.T.J., this issue, p. 1505.